Micromachining for Optical and Optoelectronic Systems

MING C. WU, MEMBER, IEEE

Invited Paper

Micromachining technology opens up many new opportunities for optical and optoelectronic systems. It offers unprecedented capabilities in extending the functionality of optical devices and the miniaturization of optical systems. Movable structures, microactuators, and microoptical elements can be monolithically integrated on the same substrate using batch processing technologies. In this paper, we review the recent advances in this fast-emerging field. The basic bulk- and surface-micromachining technologies applicable to optical systems are reviewed. The free-space microoptical bench and the concept of optical prealignment are introduced. Examples of micromachined optical devices are described, including optical switches with low loss and high contract ratio, low-cost modulators, micromechanical scanners, and the XYZ micropositioners with large travel distance and fine positioning accuracy. Monolithically integrated systems such as single-chip optical disk pickup heads and a femtosecond autocorrelator have also been demonstrated.

Keywords*—*Integrated optics, integrated optoelectronics, microelectromechanical devices, optical switches.

I. INTRODUCTION

The miniaturization and integration of electronics have created a far-reaching technological revolution. The invention of integrated circuits not only allows a large number of transistors to be fabricated on the same silicon chip but also enables them to be interconnected into functional circuits. Today, the optics is at the same stage that electronics was a couple of decades ago: though high-performance optoelectronic devices have been developed, most of the optical systems are still assembled piece by piece. In 1969, Miller proposed the concept of "integrated optics" [1], in which he envisioned active optical devices interconnected by optical waveguides, similar to the way transistors are interconnected by wires in integrated circuits. Though there has been significant development of waveguide-based integrated optics (also known as photonic integrated circuit), many free-space optical systems cannot be integrated by such technology. Free-space optics can perform optical imaging and generate diffraction-limited focused spots, and is widely used in optical display, data storage, switching, and sensing systems.

The micromachining, or microelectromechanical systems (MEMS) [2], technology has opened up many new possibilities for free-space optical systems. Movable micromechanical structures as well as precision optomechanical parts can be made by micromachining—a batch-fabrication technology similar to the microfabrication process for making very large scale integrated (VLSI) circuits. The movable structures are attractive for optical applications because small mechanical displacement can often produce physical effects that are stronger than the conventional electrooptic or free carrier effects. For example, a displacement of one-quarter wavelength in an interferometer can produce an ON/OFF switching. Many new optical devices and systems based on movable structures have been reported. Compared with macroscale optomechanical devices, the micromechanical devices are smaller, lighter, faster (higher resonant frequencies), and more rugged. Very efficient light modulators, switches, broadly tunable semiconductor lasers, detectors, and filters can be realized by the optical MEMS technology [3], [4]. The optical MEMS technology is sometimes also called microoptoelectromechanical systems (MOEMS) or microoptomechanical systems (MOMS). In this paper, we will use these terms interchangeably.

Optics is an ideal application domain for the MEMS technology: photons have no mass and are much easier to actuate than other macroscale objects. Microactuators with small force and medium travel distance are useful for many optical applications. Packaging of optical MEMS devices may also be easier than that of other MEMS devices since optics provides a noncontact, nonintrusive access to the MEMS devices. Its applications include projection and head-mount display, optical data storage, printing, optical scanners, switches, modulators, sensors, and packaging of

Manuscript received July 13, 1997; revised August 5, 1997. This work was supported in part by the Defense Advanced Research Project Agency under Grant DABT63-95-C-0050 and in part by the Packard Foundation under Grant 92-5208.

The author is with the Electrical Engineering Department, University of California, Los Angeles, CA 90095-1594 USA (e-mail: wu@ee.ucla.edu).

Publisher Item Identifier S 0018-9219(97)08236-4.

0018–9219/97$10.00 © 1997 IEEE

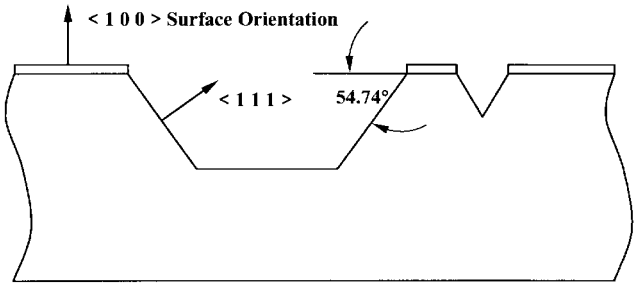

(a)

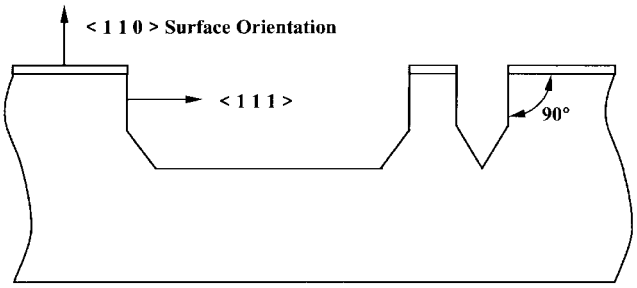

(b)

Fig. 1. Schematic diagrams illustrating the profiles of anisotropically etched silicon substrates. (a) (100). (b) (110).

optoelectronic components. The marriage of optics and MEMS has created a new class of microoptoelectromechanical devices and integrated circuits that are more efficient than macroscale devices.

II. Micromachining Technology for Optical Applications

A. Bulk Micromachining

Bulk micromachining has long been employed to create three-dimensional optomechanical structures on silicon substrate for aligning optical fibers or forming microoptical elements [5]. Single crystal silicon has excellent mechanical properties, and silicon substrates with high purity are readily available at low cost for semiconductor manufacturing. Silicon can be machined precisely by anisotropic etchants, whose etching rates depend on the crystallographic orientations [5], [6]. The etching rate of anisotropic etchants, such as ethylene diamine pyrocatechol (EDP), potassium hydroxide (KOH), and tetramethylammonium hydroxide (TMAH), is much slower in the <111> directions than in the <100> and <110> directions. Selectivity, defined as the ratio of the etch rates of the desired direction to those of the undersized one, for such anisotropic etchants can be higher than 100. This is a very powerful technique to create three-dimensional optomechanical structures with high precision.

Silicon V-grooves are now widely used in optical instruments and packaging of fiber and optoelectronic components [7], [8]. They are created by anisotropic etching of a (100) silicon substrate with stripe openings along the <110> or <1$\bar{1}$0> directions. The exposed {111} planes form a 54.74° slope with the surface of the wafer, as shown in Fig. 1(a). The depth of the V-groove can be very well controlled by lithography because {111} planes are effective stop-etching planes. Pyramidal-shaped holes that are ideal for holding ball lenses can also be formed by etching through square openings. These V-grooves and the pyramidal-shaped holes form the basis of conventional microoptical benches. As shown in Fig. 2(a), bulk optical components are dropped onto the etched silicon substrates and precisely positioned by holes of various geometry. Vertical micromirrors can be formed by anisotropic etching on a (110) silicon substrate [5], [6], as shown in Fig. 1(b). The atomically smooth {111} planes are perpendicular to the surface of the substrate and provide large-area, optical-quality surfaces. The selectivity of {110} over {111} planes is as high as 500 for some KOH solutions. Therefore, high-aspect-ratio microstructures can be produced this way. Micromirrors with 2-μm thickness and 200-μm height have been reported [9]. These vertical micromirrors are semitransparent and can be used as beam splitters. Fig. 2(b) illustrates the optical circuits consisting of such thin micromirrors, including Fabry–Pérot and Michaelson interferometer [9]. In addition to the {111} stop etch planes, some silicon etchants exhibit reduced etch rate in regions that are heavily doped with boron, adding more flexibility in defining the final shapes of the structures [5]. The boron diffusion therefore can be utilized to pattern membranes, suspended beams, or support beams for the vertical mirrors etched on (110) silicon substrate [10].

The vertical micromirrors created by anisotropic etching of (110) silicon substrates are, however, orientation dependent. Recently, there has been significant interest in three-dimensional structures created by deep reactive ion etching (DRIE) [11], [12]. DRIE allows etching of highly anisotropic, randomly shaped and located features into a single crystal silicon wafer, with only photoresist as an etch mask. Fig. 3 shows the scanning electron micrograph (SEM) of three-dimensional structures etched by DRIE [12]. Though the etched surface is rougher than the wet chemically etched (110) wafer, it is still smooth enough for many micromirror applications. Marxer *et al.* [13] and Juan *et al.* [14] have used the DRIE technique to fabricate a vertical micromirror for fiber-optic switches. The microactuators for the switch are also integrated through the same DRIE process. The mirror roughness is estimated to be 36 nm, which corresponds to a scattering loss of 6% [13].

B. Surface Micromachining

In contrast to bulk micromachining, in which substrate materials are removed to create three-dimensional structures, surface-micromachined structures are constructed entirely from deposited thin films. Alternating layers of *structural* and *sacrificial* materials are deposited and patterned on the substrate. The sacrificial materials can be selectively removed by an etchant that attacks only the sacrificial materials. Suspended beams, cantilevers, diaphragms, and cavities can be made this way. The use of sacrificial material to free micromechanical devices from the silicon

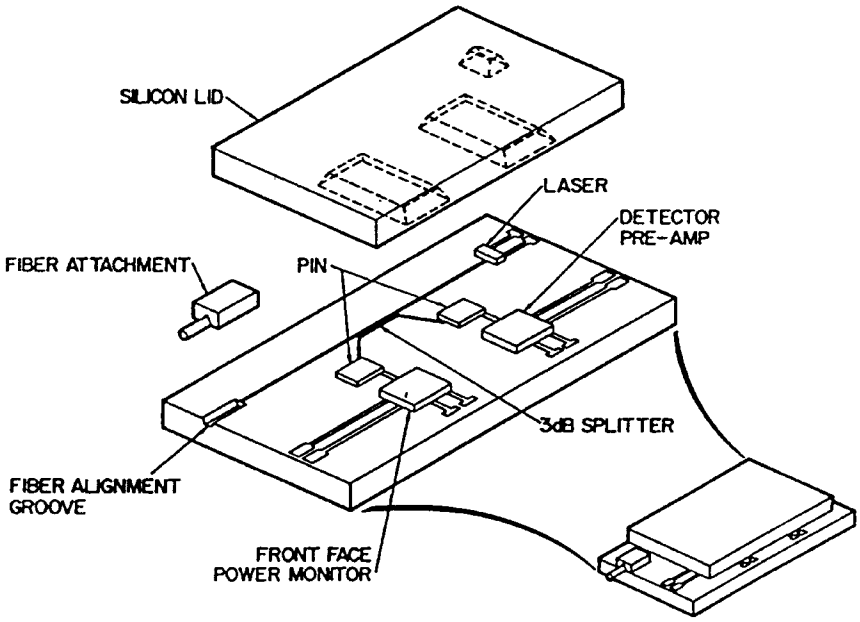

(a)

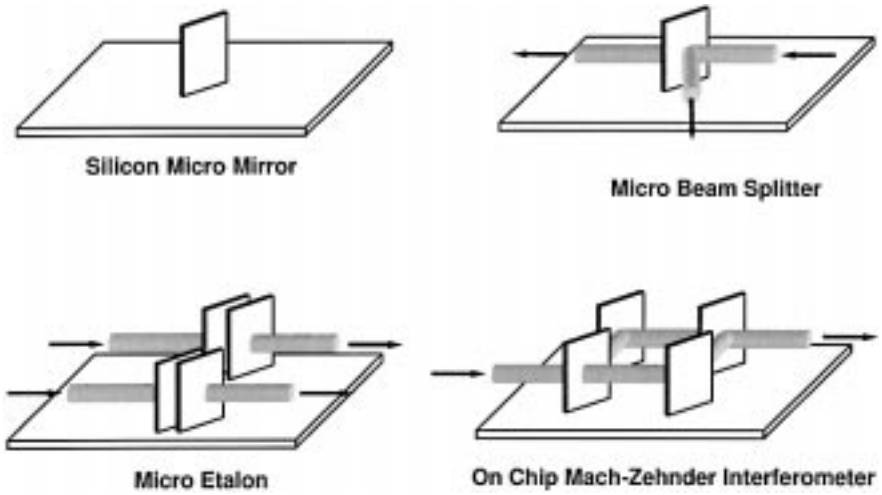

(b)

Fig. 2. Silicon optical benches on silicon substrates. (a) (100) [7]. (b) (110) (after [9]).

substrate was first demonstrated by Nathanson *et al.* [15] for fabricating a field effect transistor with a suspended resonant gate. In 1983, Howe and Muller [16] described the use of polysilicon as the structural material and silicon dioxide as the sacrificial material. Because of the excellent mechanical properties of polysilicon material and the high selectivity of sacrificial etching with hydrofluoric acid, this combination has become the most popular choice for surface micromachining.

Fig. 4 illustrates the surface-micromachining process for making cantilevers. This process requires one layer of sacrificial material and one layer of structural material. The complexity of the surface-micromachining process can be quantified by the number of structural and sacrificial materials. With two structural polysilicon layers, free-moving mechanical gears, springs, and sliders have been demonstrated [17], [18]. Micromotors [19], [20] and other microactuators were later demonstrated using similar fabrication processes. One of the main features that distinguishes the surface micromachining from the bulk micromachining is that many different devices can be fabricated using a common fabrication process. By changing the patterns on the photomask layouts, different devices such as cantilever resonators, sliders, micromotors, or comb drive actuators are fabricated simultaneously on the same substrate. This methodology is similar to that used in today's VLSI circuits. For this reason, the surface-micromachining process is often referred to as an integrated circuit (IC) process or VLSI-like process. Today, there already are two commercial foundries offering such polysilicon surface-micromachining processes.[1] Some of these processes can also be integrated

[1]MEMS Technology Applications Center, Microelectronics Center at North Carolina (MCNC), Research Triangle Park, NC, and Integrated Micro Electro Mechanical Systems, offered at Analog Devices, Cambridge, MA.

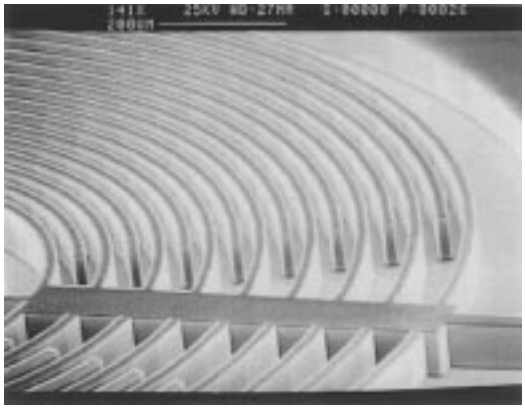

Fig. 3. The SEM micrograph of high-aspect-ratio structures created by DRIE [12].

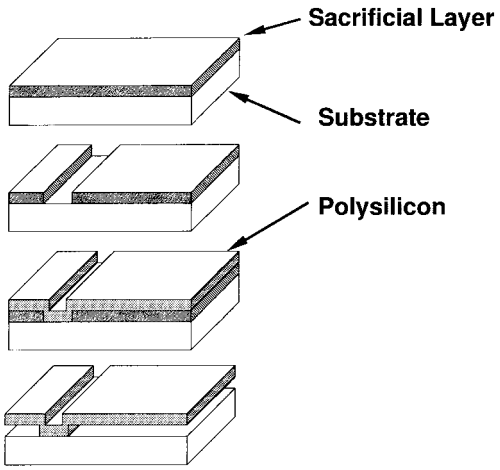

Fig. 4. Schematic of the fabrication process for surface-micromachined cantilevers.

with complementary metal–oxide–semiconductor circuits [21], [22]. Surface micromachining using other combinations of structural/sacrificial materials has also been demonstrated. For example, aluminum structure material and organic sacrificial material are used in Texas Instruments' digital micromirror devices (DMD's) [23], which will be discussed later.

C. Microhinges

Out-of-plane structures with high aspect ratios are often needed for free-space optical systems. Though they can be obtained by anisotropic etching or deep dry etching, it is difficult to pattern their side walls, as often required for free-space optical elements. In 1991, Pister and his coworkers proposed using the *microhinges* to fabricate a variety of three-dimensional structures using the surface-micromachining process [24]. This allows the surface-micromachined polysilicon plates to be patterned by photolithography and then folded into three-dimensional structures. The schematic cross section and the fabrication processes of the microhinge are illustrated in Fig. 5. It consists of a hinge pin and a confining staple. After selective etching of the sacrificial silicon dioxide, the polysilicon plate connected to the hinge pin is free to rotate out of the substrate plane and become perpendicular to the substrate. It is also possible to achieve other angles for the polysilicon plates. The microhinge technology allows the three-dimensional structures to be monolithically integrated with surface-micromachined actuators. It is particularly useful for fabricating integrable free-space microoptical elements, as will be shown in the next section.

In addition to the microhinges, alternative surface-micromachining techniques have been proposed for fabricating three-dimensional structures. The research group at the University of Tokyo proposed to use the "reshaping" technology to create complex three-dimensional structures [25]. The basic concept is to use thin flexure beams to connect polysilicon plates. The beams are then buckled or twisted by integrated microactuators to create the desired three-dimensional structures. By passing current through the polysilicon beam until plastic deformation, the three-dimensional structures are permanently fixed. Other techniques have also been proposed. Green *et al.* proposed to use the surface tension of molten solder to produce out-of-plane rotation [26]. Smela *et al.* used active polymers for controlled folding of microstructures in electrolyte liquid solution [27].

III. Free-Space Microoptical Bench

These surface-micromachining techniques have opened up the possibility of monolithically integrating free-space microoptical elements, micropositioners, and microactuators on the same substrate. This new technology, called *free-space microoptical bench* (FS-MOB), is illustrated in Fig. 6 [28]. In free-space optical systems, photons propagate between optical elements without being confined in physical media. Normally, the free-space optical systems are constructed on optical tables, with each optical element mounted on an XYZ micropositioning stage for optical alignment. With the micromachining technology, the optical system can be miniaturized and batch fabricated on a silicon substrate. Unlike the conventional systems, the optical elements can be integrally fabricated on translation or rotation stages. Microactuators for moving the optical elements can also be fabricated by the same micromachining process.

FS-MOB offers many advantages over conventional optical systems. First, the FS-MOB is made by a VLSI-like batch-fabrication process, which can significantly reduce the system cost. Conventional optical systems often need custom design and expensive assembly. Second, the optical system can be miniaturized by the FS-MOB technology. Many optical systems are limited by the sizes of micropositioning stages and optomechanical structures. Using the MEMS structures and actuators in FS-MOB, the size and weight of the optical systems can be greatly reduced. Third, the entire optical system can be monolithically integrated on a single chip. The use of out-of-plane optical elements allows multiple elements to be cascaded along the optical axes on the same substrate. Therefore, single-chip microoptical systems can be achieved. Fourth, the optics in FS-MOB can be "prealigned." Since all the microoptical

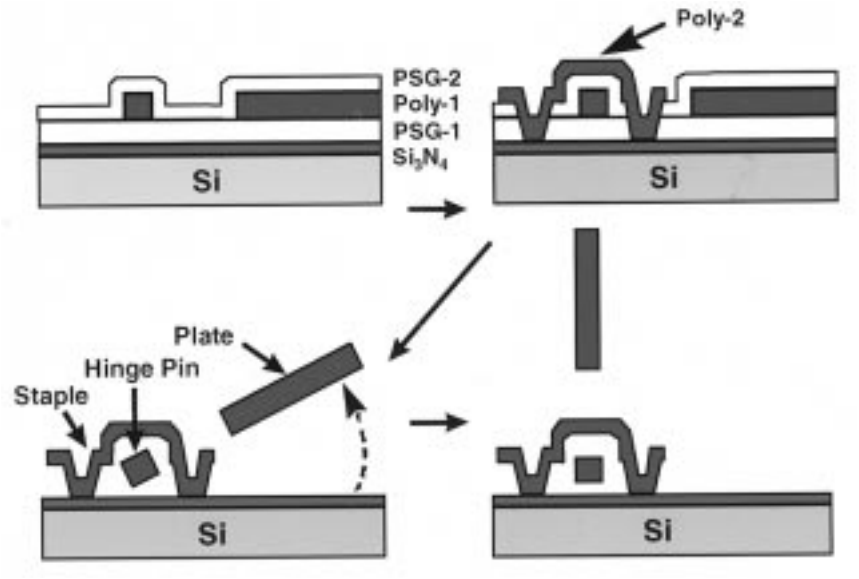

Fig. 5. Schematic of the fabrication process for surface-micromachined microhinges (after [24]).

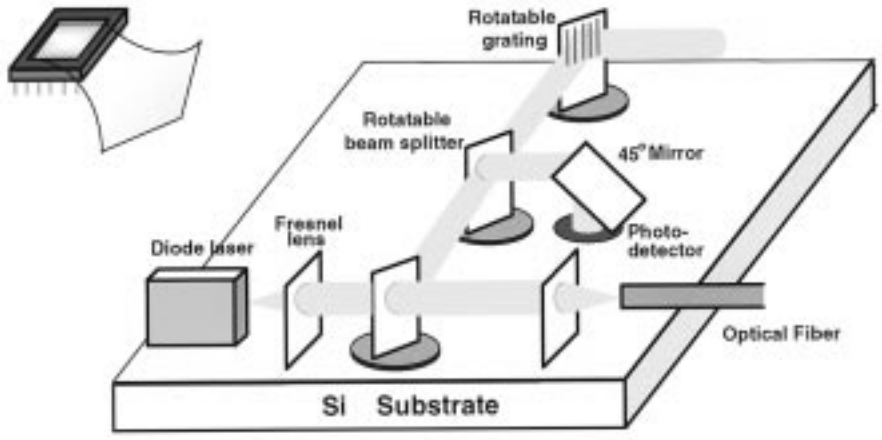

Fig. 6. Schematic illustrating the concept of FS-MOB. Microoptical elements, micropositioners, and microactuators are monolithically integrated on silicon substrate by surface micromachining.

elements and the optomechanical structures are made at the same time by the photolithographic processes, they can be aligned during layout of the photomasks. The accuracy of the alignment is limited by the misalignment error of photolithography and the mechanical clearance between the movable structures, which is on the order of a micrometer. Fine optical alignment ($< 0.1\ \mu$m) can be achieved by on-chip microactuators. The integrated microactuators also allow dynamic tracking of alignment. The optical prealignment enables the "interconnections" between optical elements to be fabricated at the same time as the optical elements. This allows a functional optical system to be monolithically integrated and aligned on a single chip. This is similar to the concept of VLSI, in which the interconnections between transistors are fabricated monolithically. Combining the large number of transistors and the monolithic interconnections, highly functional electronic systems such as microprocessors have been produced.

FS-MOB represents a paradigm shift for the optical systems. The conventional optical system is assembly intensive. The optical elements are made separately and then assembled into optical systems. FS-MOB resembles more the VLSI systems: it is design intensive, and the same standard process is used to fabricate different functional circuits. It is based on batch processing techniques and is more suitable for mass production. In the following, we describe the basic building blocks of FS-MOB.

A. Diffractive Microlenses

Diffractive microlenses are very attractive for integrating with FS-MOB because:

1) their focal length can be precisely defined by photolithography;
2) microlenses with a wide range of numerical apertures (F/0.3–F/5) can be defined;
3) microlenses with diameters as small as a few tens of micrometers can be made;
4) their thickness is on the order of an optical wavelength [29]–[31].

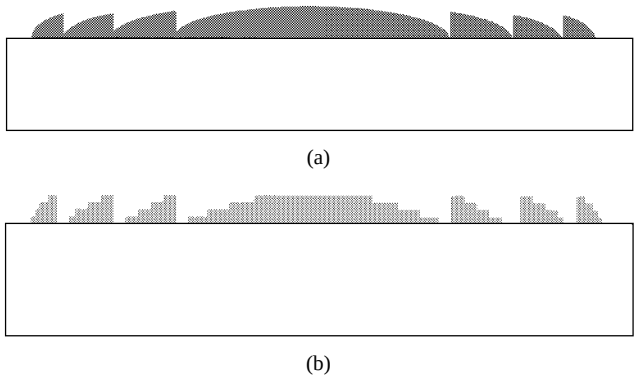

Fig. 7. (a) Schematic of a Fresnel zone plate. (b) Schematic of a multiple-level binary microlens.

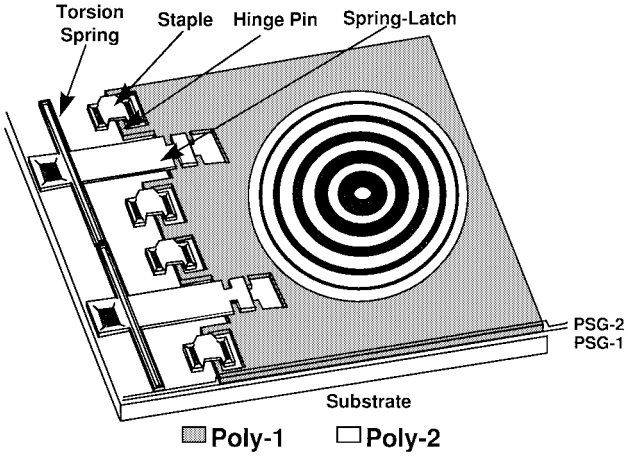

Fig. 8. Schematic of the out-of-plane micro-Fresnel lens fabricated on a hinged polysilicon plate.

The thin construction is particularly suitable for the surface-micromachining process because the thicknesses of the structural layers are only on the order of 1 μm. Fig. 7 shows the schematic diagram of two diffractive microlenses: (a) Fresnel lens and (b) multiple-level binary microlens. The binary-amplitude Fresnel zone plate has alternating transmission and blocking zones. Though it is very easy to fabricate, however, its efficiency (diffraction efficiency into the first-order beam) is limited to 10%. The efficiency of a binary microlens with $M = 2^m$ phase levels is [29]

$$\eta = \left[\frac{\sin(\pi/M)}{\pi/M}\right]^2.$$

The efficiency increases with the number of phase levels at the expense of more complicated fabrication processes. For example, $\eta = 41\%$ for $M = 2$, $\eta = 81\%$ for $M = 4$, and $\eta = 99\%$ for $M = 16$. Fabrication of binary microlenses on various substrates has already been demonstrated [29]–[31]. These microlenses are usually confined to the surface of the substrates.

Microlenses with optical axes parallel to the substrate are necessary for single-chip microoptical systems. This is achieved by combining the conventional microoptics technology with the surface-micromachined microhinges. As shown in Fig. 8, the micro-Fresnel lens is fabricated on a hinged polysilicon plate [32], [33]. Since the polysilicon plate lies on the surface of the substrate before assembly, conventional planar fabrication technology can be used to define the patterns of the Fresnel lens. After releasing etch, the micro-Fresnel lens plate is rotated out of the substrate plane and becomes perpendicular to the substrate. The assembly process is illustrated in Fig. 9. To enhance the mechanical strength and to more precisely define the angle of the microlens, a pair of side support plates is added. The side support plates are also made on polysilicon using the microhinge technology. They have a V-shaped opening at the top, followed by a long, narrow groove in the center. When they are folded onto the microlens plate, the 2-μm-thick microlens plate is firmly locked into the 2.5-μm-wide groove. As will be shown later, the side support plates play a critical role in the robustness of such three-dimensional microstructures. The maximum angular variation of the microlens depends on the geometry of the side support plates. Angular variation of less than 0.1° is achievable. Fig. 10 shows the SEM micrograph of a micro-Fresnel lens with a diameter of 280 μm, a focal length of 500 μm, and an optical axis of 254 μm above the silicon surface [33]. For simplicity, only a binary-amplitude Fresnel zone plate

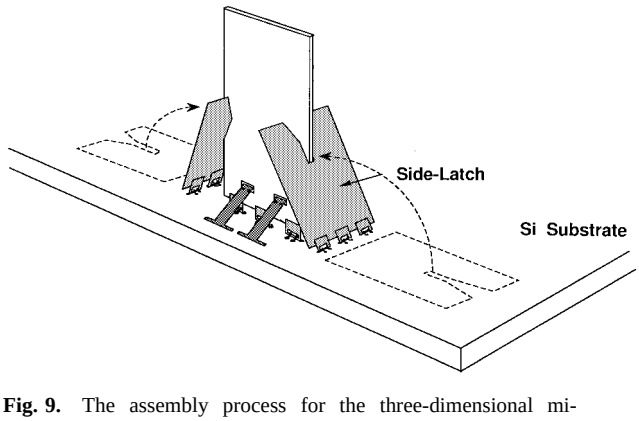

Fig. 9. The assembly process for the three-dimensional micro-Fresnel lens.

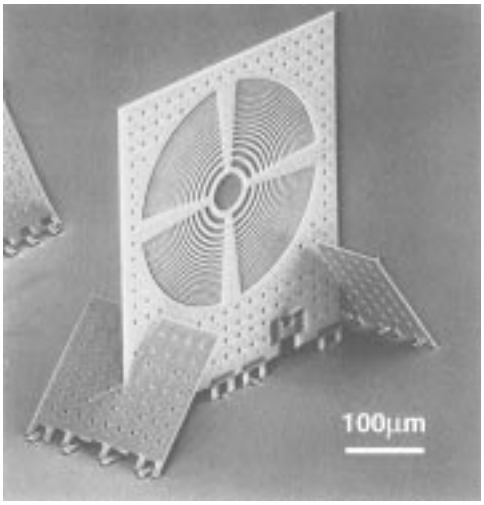

Fig. 10. The SEM of the out-of-plane micro-Fresnel lens. The lens has a diameter of 280 μm, a focal length of 500 μm, and an optical axis of 254 μm above the silicon substrate.

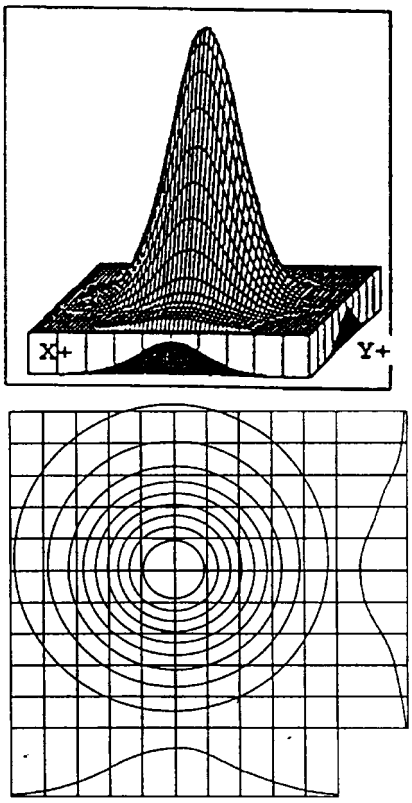

Fig. 11. The intensity profile and contour plot of the optical beam emitted from an optical fiber and collimated by the micro-Fresnel lens.

is demonstrated. Lenses as large as 650 μm and as tall as 1.4 mm also have been demonstrated [32].

The lens exhibits very good optical performance. The output beam from a single-mode fiber is successfully collimated by the lens [32]. Fig. 11 shows the intensity profile of the collimated beam and the contour plot of the intensity distribution. Very good agreement with Gaussian shape is obtained. The intensity full-width-at-half-maximum (FWHM) divergence angle of the collimated beam has been reduced from 5.0° to 0.33°. The diffraction efficiency of the micro-Fresnel lens was measured to be 8.6% using the method described by Rastani *et al.* [30]. This is in agreement with the theoretical limit of the binary-amplitude Fresnel zone plate. As mentioned earlier, efficiency greater than 80% can be achieved by multilevel Fresnel lenses at the expense of more complicated fabrication processes. Another potential issue of fabricating diffractive optical elements on the surface-micromachined polysilicon plates is the surface roughness. The plates might need to be smoothened by chemical-mechanical planarization, which can reduce the surface roughness to 17 Å [34]. Another alternative to achieve high efficiency is to use a refractive lens, as described in the next section.

B. Refractive Microlenses

The refractive microlenses are complementary to the diffractive microlenses. They offer several advantages over diffractive optical elements. Their focal length is independent of the optical wavelength (except a weak dependence due to the dispersion of the lens material). It is also easier to make fast refractive microlenses without tight critical dimension control. Refractive microlenses do not suffer from diffraction loss, and it is easier to make a high-efficiency lens at low cost. In contrast, high-efficiency diffractive microlenses need multiple critical lithography steps.

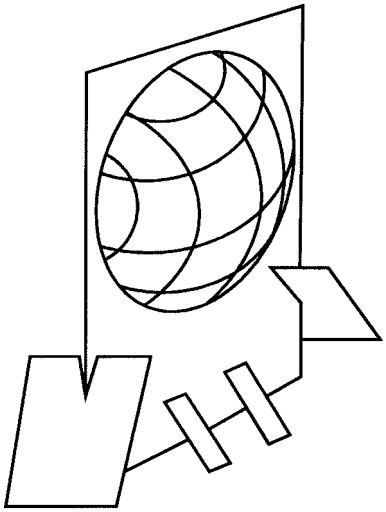

Fig. 12. Schematic of an out-of-plane refractive microlens.

Fabrication of a planar refractive microlens array on semiconductor and dielectric substrates has been demonstrated using photoresist/polyimide reflow techniques [35]–[38]. The lens pattern can also be transferred to substrate through reactive ion etching or ion milling. Here, we combine the planar refractive microlens fabrication with the surface-micromachining process to create low-cost, high-quality out-of-plane refractive microlenses. Fig. 12 shows the schematic drawing of the out-of-plane refractive spherical lens [39]. One potential issue for such microlenses is the scattering loss of the supporting polysilicon plate. The scattering loss is related to the surface roughness by [13], [40]

$$\beta = 1 - e^{-(4\pi\sigma \cos \theta_i/\lambda)^2}$$

where β is the percentage of the scattering loss, σ is the root-mean-square roughness of the polysilicon surface, θ_i is the incident angle, and λ is the optical wavelength. The surface roughness of as-grown polysilicon is on the order of 45 nm (the exact value depends on the deposition condition), and the corresponding scattering loss is 17% per interface at 1300-nm wavelength. There are two approaches to reducing the scattering loss. The first is to smooth the surface by chemical-mechanical planarization (CMP). The surface roughness can be reduced to 1.7 nm, which will improve the scattering loss to 0.02%. Both surfaces need to be polished for a transmission device, however, and it is difficult to polish the bottom side of the polysilicon plate. Alternatively, we can remove the polysilicon material at the center of the lens, which forms an aperture for the

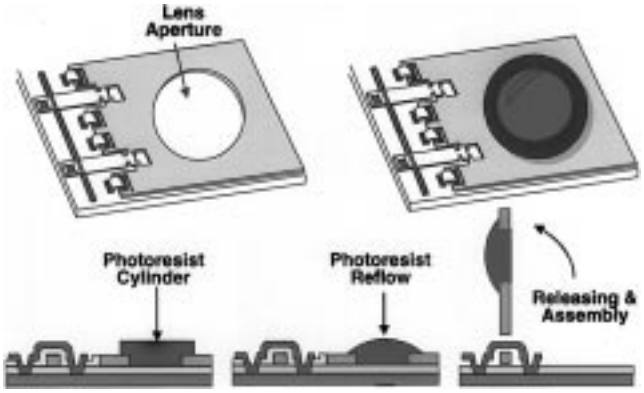

Fig. 13. The fabrication process for the three-dimensional refractive microlens. The microlens is fabricated on a hinged polysilicon plate by the reflow technique.

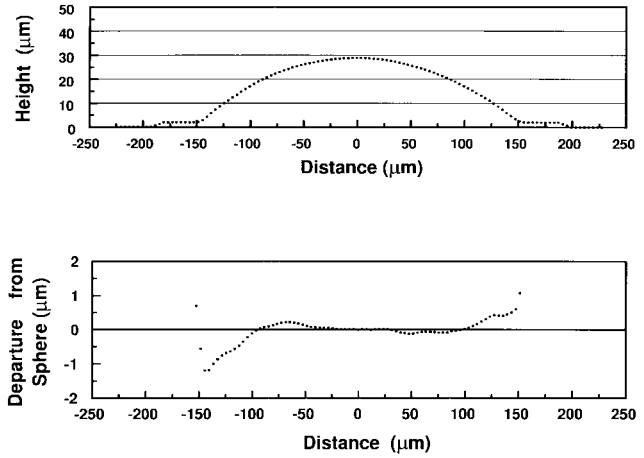

Fig. 14. The surface profile of the microlens. The lens is 30 μm thick at center and 300 μm in diameter.

microlens. The scattering as well as reflection loss of the polysilicon plate are thus eliminated. We have adopted the second approach here.

The fabrication process is illustrated in Fig. 13 [39]. First, a lens mount is fabricated using the surface-micromachining technique. This process is similar to that of the micro-Fresnel lens except that an aperture is etched in the center of the polysilicon plate. Before releasing, a 20-μm-thick AZ 4620 photoresist cylinder is deposited on the hinged polysilicon plate. The lens is realized by heating the photoresist cylinder to 200°C, causing the photoresist to reflow into a spherical shape. Fig. 14 shows the surface profile of the reflowed photoresist. The lens is 30 μm thick at center, and the maximum deviation from spherical is less than 0.5 μm to within 5 μm of the edges. The resulting lens has a diameter of 300 μm and a focal length of 670 μm. Refractive microlenses with an F-number ranging from one to five and diameters from 30 to more than 500 μm can be made by this technique. The microlens can be made vertical to the substrate by rotating the supporting polysilicon plate after the reflow processes. Fig. 15 shows the SEM micrographs of both the front and back sides of the microlens. The back-side view clearly shows the aperture of the microlens. The optical loss of the microlens is measured

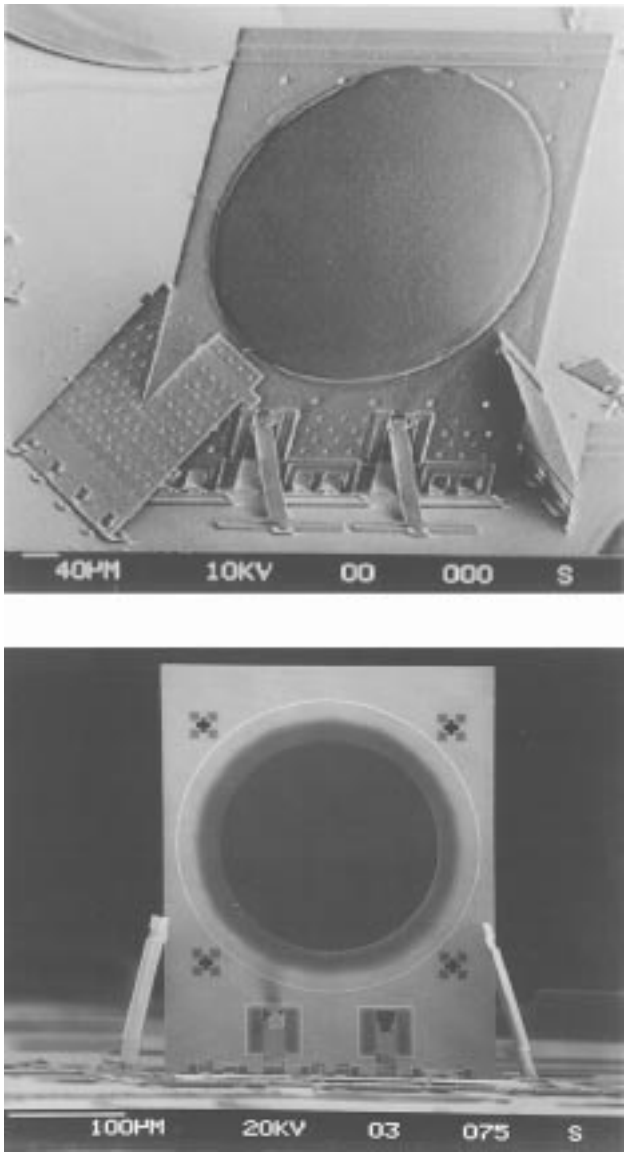

Fig. 15. SEM micrographs of the front and back sides of the three-dimensional refractive microlens. The aperture of the microlens is clearly visible from the backside.

to be 0.7 dB at 632-nm wavelength. Lower loss is expected at longer wavelengths. The optical axis of the microlenses is fixed to the same height as the rest of the FS-MOB by photolithography. Therefore, the refractive microlens can be aligned to other optical elements to within the fabrication tolerance.

Very good optical performance has been achieved for the refractive microlens. The divergence angle of the light emitted from a single-mode fiber at 630 nm has been reduced from 3.3° to 0.18° after it is collimated by the refractive microlens. The intensity contour of the collimated beam is also very symmetric, as shown in Fig. 16, indicating the high quality of the spherical microlens.

C. Micropositioners

As described in [17] and [18], various types of movable structures can be made by the surface-micromachining

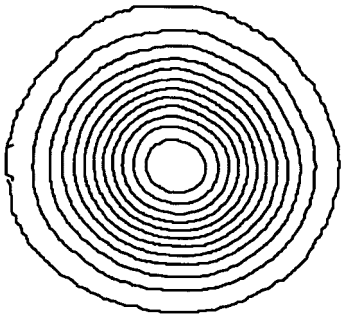

Fig. 16. The intensity contour of the optical beam collimated by the spherical microlens.

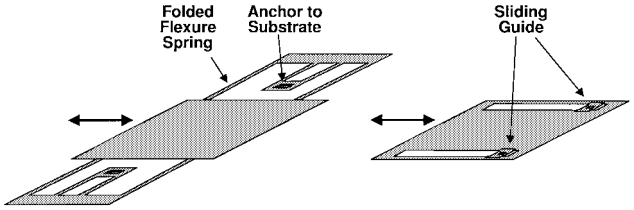

Fig. 17. Surface-micromachined translation stage with (a) flexure springs and (b) sliding guides.

technique. A linear translation stage and rotation stage can be built in a similar way on FS-MOB. The microlenses and other out-of-plane microoptical elements can be integrated with translation and rotation stages by attaching the microhinges to a movable polysilicon plate. The movable stage consists of a fully released polysilicon plate that is attached or confined to the substrate by either 1) flexure springs or 2) sliding guides. Fig. 17 illustrates these two types of micropositioners. The spring-attached stage is more accurate; however, it has limited travel distance. The spring restoring force also needs to be constantly balanced by the actuators. The sliding type of stage has a long travel distance. Since there is no restoring force, the friction between the stage and the substrate or the sliding guides can hold the stage in place without any power consumption. On the other hand, the finite clearance between the stage and the sliding guides may cause some statistical variation and hysteresis. These two types of stages are complementary.

To integrate the microoptical elements on translation stages, the microoptics plate now needs to be constructed on the second polysilicon layer and connected to the microhinges defined on the first polysilicon layer. The bases of the spring latched and staples are now connected to the movable plate on the first polysilicon layer instead of the substrate. Fig. 18 shows the SEM micrograph of a three-dimensional micrograting integrated on a rotation stage [41]. The stage in the SEM has been rotated by 20°. The rotary grating has been employed to build an integrated-wavelength meter for a single-wavelength laser [42] and microspectrometer [43].

D. Microactuators

Perhaps the most interesting feature of micromachined optics is the ability to integrate microactuators with the optical elements. Many new surface-micromachined microactuators have been proposed and demonstrated since the invention of micromotors. It is beyond the scope of this paper to have a complete review of these microactuators. Here, we will describe only a selected set of microactuators that are particularly useful for optical applications. Fig. 19 shows the schematic drawing of these actuators.

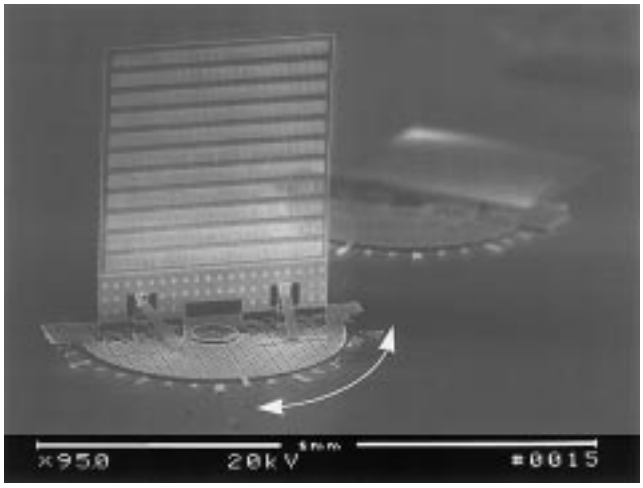

Fig. 18. SEM micrograph of a three-dimensional micrograting integrated on a rotation stage.

1) Comb Drive Actuator [44], [45]: The comb drive is actuated by electrostatic force between a pair of movable combs and fixed combs, as shown in Fig. 19(a). When a voltage is applied, the movable comb is attracted to the stationary comb. The position of the movable comb can thus be controlled by voltage. This is perhaps by far the most popular surface-micromachined actuator. Typical surface-micromachined polysilicon comb drive actuators can produce micronewtons of force and a few micrometers of displacement. The comb drive actuators have been employed to drive optical choppers [46] and bar-code scanners [47]. Another electrostatic actuator is gap-closing actuators [48], [49]. They have larger force but smaller displacement.

2) Linear Microvibromotor [50], [51]: Impact actuation can be used to obtain relatively large motion from small-displacement resonant structures such as comb drive actuators. The linear microvibromotor shown in Fig. 19(b) consists of two 45° resonant comb drives, two −45° resonant comb drives, and a slider. Upon each impact from the comb drives, the slider moves by an average step size of 0.27 μm [51]. The standard deviation of the step size is relatively large (0.17 μm) due to the impact actuation and wobble of the slider. The position and speed of the slider can be controlled by adjusting the number of impacts. A maximum speed of 1 mm/s has been achieved. The linear microvibromotor has been used to actuate a slide-tilt mirror for alignment for optical beams for fiber coupling [52].

3) Stepper Motor: In addition to impact actuation, the long travel distance of the slider can also be achieved by the "hold-and-pull" actuation [53], [54]. A large-force, small-displacement actuator, such as the gap-closing actuator, first

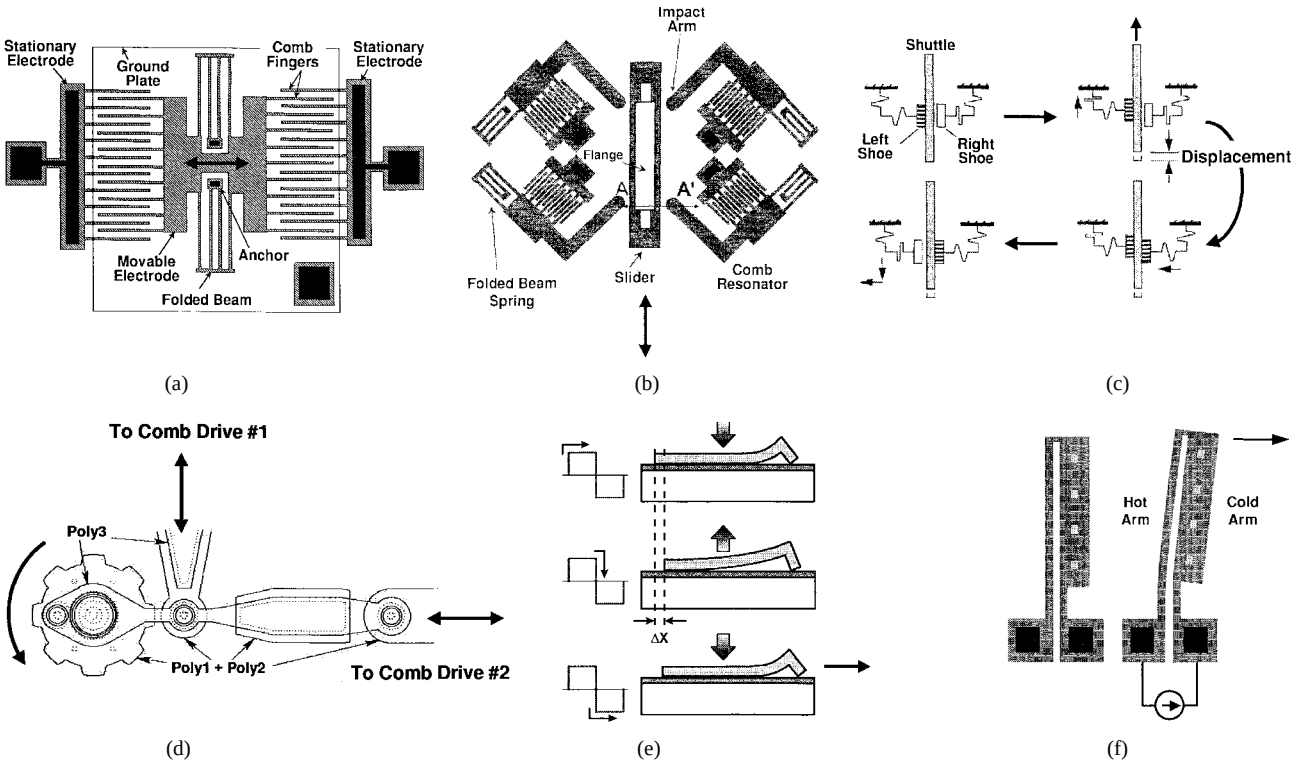

Fig. 19. Schematic of microactuators commonly used in surface-micromachined optical systems. (a) Comb drive actuator [44], [45]. (b) Linear microvibromotor [50], [51]. (c) Stepper motor [53], [54]. (d) Microengine [55], [56]. (e) Scratch drive actuator [59], [60]. (f) Thermal actuator [65], [66].

contacts and holds the slider. Then an orthogonal actuator connected to the first actuator pulls the slider forward by 2 μm. The actuator arrays can be on both sides of the slider for alternating "hold-and-pull" actuation, as illustrated in Fig. 19(c).

4) Microengine [55], [56]: Sandia National Laboratory, NM, has demonstrated a microengine that utilizes two orthogonal actuator arrays to drive a rotating output gear [Fig. 19(d)]. Its principle is similar to two orthogonal pistons connected to a crankshaft in an internal combustion engine. The output gear could then be coupled to other gears for delivering the drive power. The microengine is capable of very high angular speed (up to millions of revolutions per minute) and has been applied to drive optical shutters [57] and other optical components and micropositioners [58].

5) Scratch Drive Actuator (SDA) [59], [60]: The SDA consists of a polysilicon plate with a vertical bushing, as shown in Fig. 19(e). It is actuated by applying pulses of electric bias between the polysilicon plate and a bottom electrode separated by an insulating layer. When the bias is applied, the polysilicon plate is first deformed by the electrostatic force. During the downward motion, the bushing is squeezed out by a small step. Upon releasing of the bias, the friction at the front bushing is larger than the friction at the back side of the plate. Therefore, the SDA moves forward by a small step. The average step size is extremely fine: 20–30 nm. By applying a continuous pulse train, the SDA becomes like a stepper motor except that the step size is much finer. The SDA is ideal for positioning optical elements that require accuracy below 0.1 μm. Though the step size is small, the SDA can be actuated at very high frequency. By using a 50-kHz pulse train to bias the SDA, we have achieved a linear speed of 3 mm/s. The SDA has been used to actuate a buckling beam vertical actuator [60], two-dimensional XY translation stage [61] and self-assembled three-dimensional XYZ stage [62], optical switches [63], and a variable optical delay line [64].

6) Thermal Actuator [65], [66]: Thermal expansion is a strong force, but a single-material actuator based solely on the thermal expansion of a beam usually has very small deflection. By combining a "hot" arm and a "cold" arm in a U-shaped geometry, the deflection is greatly amplified. The arms are joined at the free end, which constrains the actuators to move laterally toward the cold arm. Deflection up to 16 μm and force of 4.4 μN have been obtained for the polysilicon thermal actuators at 10 mW driving power. The area is also very compact ($\sim$ 20 $\times$ 200 μm) compared with comb drive actuators. The polysilicon thermal actuator has been demonstrated to drive stepper motors and linear motors, as well as to assemble the three-dimensional structures [67].

E. Actuated Micro-XYZ Stages

The XYZ stages are the most important micropositioners in free-space optical systems for optical alignment. Optical alignment is achieved by either moving the optical beams or moving the optical elements. The former can be attained by optical beam-steering devices, while the latter requires XYZ stages.

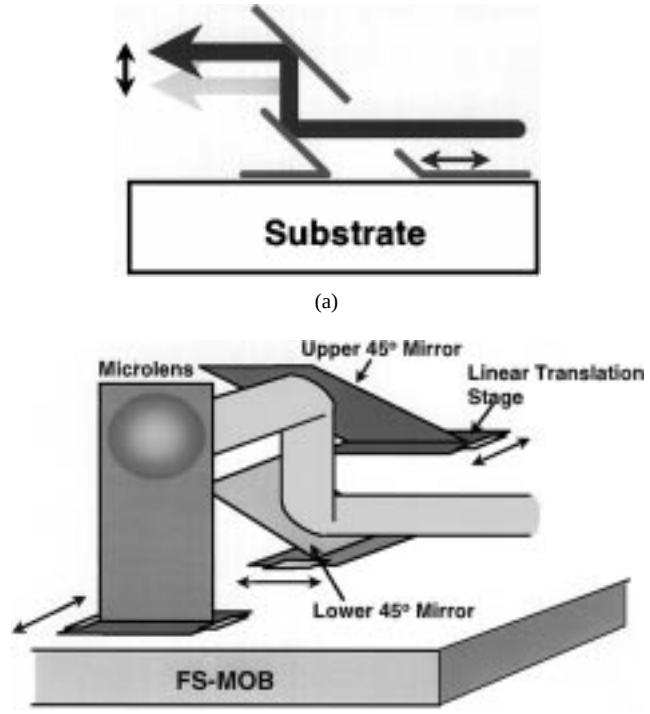

Fig. 20. (a) Schematic of vertical beam-shifting device. (b) Schematic of three-dimensional beam-steering device.

Fig. 20(a) illustrates a parallel beam-shifting device, which translates the optical beams in the lateral directions [68]. It consists of two 45° mirrors. By adjusting the spacing of the two 45° mirrors, the position of the optical beam is varied without changing the beam direction. This is useful for matching heights of the optical axes in free-space optical systems. This device can translate optical beams in either in-plane (horizontal) or out-of-plane (vertical) directions. By combining two 45° mirrors in orthogonal directions, as shown in Fig. 20(b), two-dimensional optical beam steering can be achieved [69]. By moving the lower 45° mirror, the optical beam is shifted in the horizontal direction. If the upper 45° mirror is moved, the optical beam is shifted in the vertical direction. This configuration is particularly suitable for surface-micromachined devices since only in-plane actuators are needed. The out-of-plane optical beam translation is achieved without using out-of-plane actuators. Three-dimensional optical beam alignment can be achieved by mounting the optical elements on a third translation stage that moves along the direction of the optical axis. The SEM micrograph of such a three-dimensional optical beam-steering device is shown in Fig. 21 [69]. Two-dimensional positioning of the optical beams as well as focusing/defocusing of an optical beam emitted from a single-mode fiber have been experimentally demonstrated, as shown in Fig. 22.

Another type of beam steering employs an angular scanning device. Fig. 23 illustrates a tilting/sliding mirror for two-dimensional optical alignment [52]. It consists of four polysilicon plates joined by microhinges. The micromirror plate can be tilted by moving either the front or the back

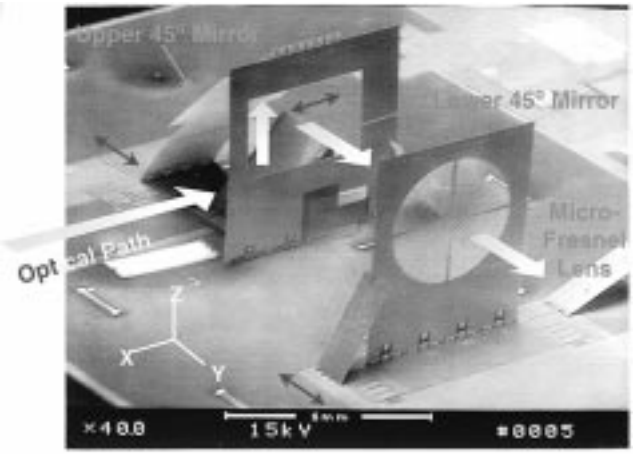

Fig. 21. SEM micrograph of the three-dimensional beam-steering device.

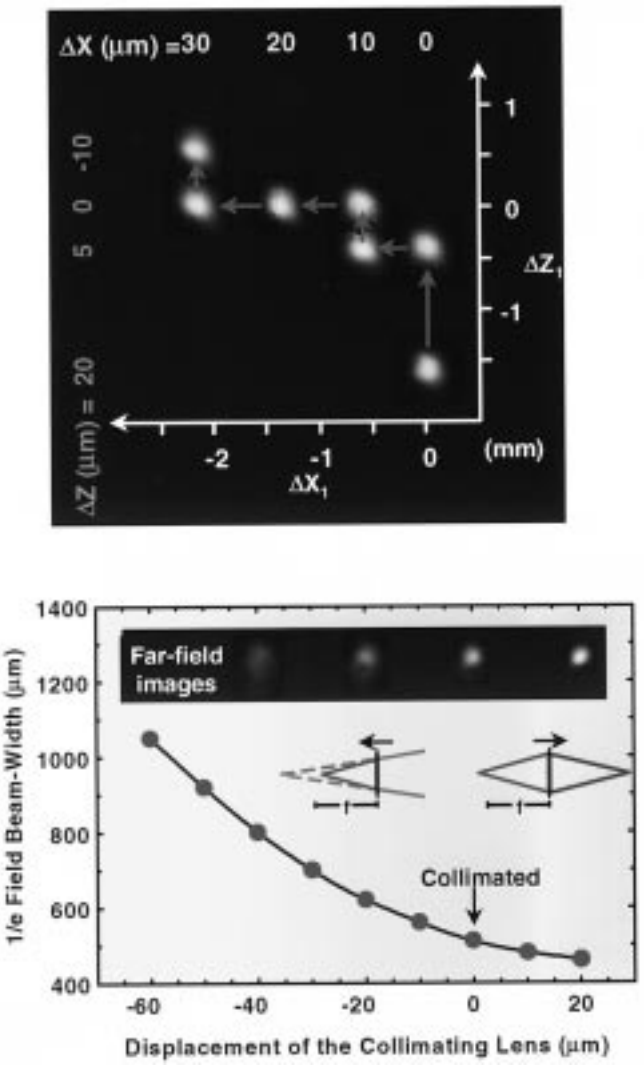

Fig. 22. Two-dimensional scanning and focusing/defocusing of the optical beams using the three-dimensional beam-steering device.

sliding plates; it can also be translated by moving both sliding plates in the same direction. If the optical beam is incident at a 45° angle, horizontal beam shifting and

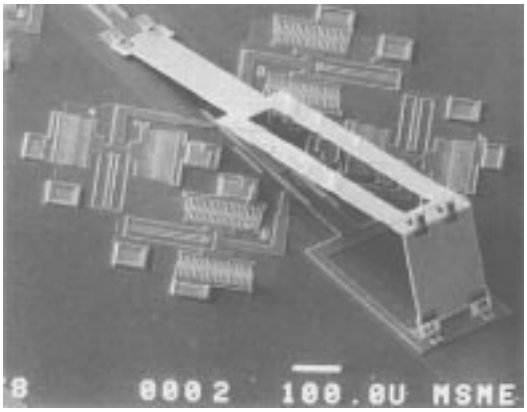

Fig. 23. A surface-micromachined sliding/tilting mirror. When the optical beam is incident at 45°, two-dimensional alignment can be achieved [52].

vertical beam scanning are achieved. The research group at the University of California, Berkeley, has used such a device for active alignment in semiconductor laser-to-fiber coupling. A coupling efficiency of 40% has been achieved [52].

In contrast to the beam-steering device, the XYZ micropositioning stages can physically move the optical elements in three directions. They are widely used in free-space optical systems. However, implementation of such XYZ stages with large travel distance and submicron accuracy is very challenging using the surface-micromachining technology. Cornell University has demonstrated a nano-XYZ stage for a scanning atomic force microscope using two sets of orthogonal comb drive actuators for XY stages and an out-of-plane torsion Z-stage [70]; the travel distance, however, is limited to below a few micrometers. A two-dimensional XY-stage was recently demonstrated by Langlet *et al.* at the University of Tokyo [61]. A suspended polysilicon plate is connected to the substrate through four flexure beams. The polysilicon plate is moved by four separate SDA's in the $\pm X$ and $\pm Y$ directions. Displacement over 40 μm has been demonstrated in all in-plane directions.

Vertical displacement is more difficult to achieve for surface-micromachined structures. Vertical comb drive has been demonstrated [71], but the displacement is limited to below 10 μm. Buckling beams have also been proposed for large out-of-plane displacement, but the vertical displacement is coupled with horizontal motion [60]. Recently, at the University of California, Los Angeles (UCLA), we have demonstrated a novel self-assembled vertical stage that can achieve large displacement with fine resolution [62]. The structure is shown in Fig. 24. It consists of five surface-micromachined polysilicon plates. The center plate is connected to four side support plates through precision microhinges. Each support plate is in turn connected to a microactuator array. Here, the SDA is chosen for this application because it can produce large displacement with fine step resolution [60]. The principle of operation for this vertical stage is shown in Fig. 25. To raise the center platform, the SDA's move in the opposite directions at

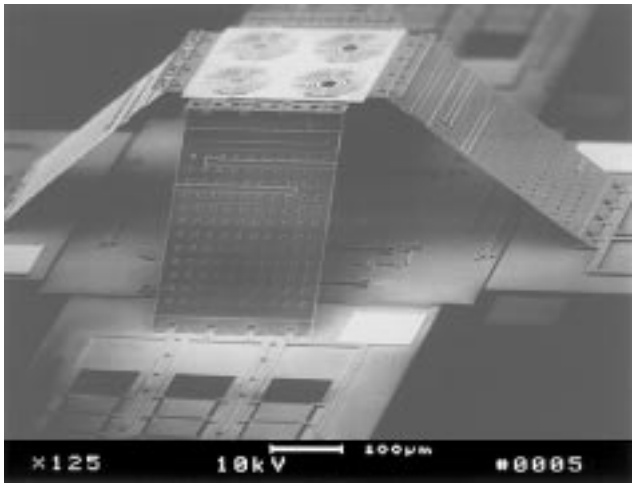

Fig. 24. SEM of a self-assembled vertical translation stage fabricated by surface micromachining. Four micro-Fresnel lenses have been integrated on the center platform. It has a large travel distance ($>$ 250 μm) and fine step size (30 nm).

the same speed. Due to the motion amplification of this structure, very large vertical displacement (250 μm) is achieved by moving the SDA's by only 110 μm. In the structure shown in Fig. 24, a micro-Fresnel lens array is monolithically integrated on the center polysilicon plate. Focusing and defocusing of surface-normal optical beams have been experimentally demonstrated using the vertical stage. It can also be made to accommodate external optical elements such as ball lenses [72]. The vertical stage can be generalized to a full XYZ stage with three degrees of freedom by incorporating sliding joints between the side support plates and the microactuators [62]. Large displacements in all three axes ($>$ 120 μm) and fine step resolution (27 nm) have been experimentally demonstrated. Another unique feature of such an XYZ stage is that it is completely self-assembled by applying electrical bias only. No manual assembly is required, which can greatly reduce the system cost. This will be discussed further in a later section.

IV. Microoptical Systems

A. Optical-Disk Pickup Head

A single-chip optical-disk pickup head has been realized by FS-MOB technology [73]. The pickup head consists of a semiconductor laser source (hybrid integrated with the help of three-dimensional alignment plates), three micro-Fresnel lenses, a beam splitter, and two 45° mirrors (Fig. 26). All the optical elements have been prealigned during the design stage. The optical beam emitted by the laser is first collimated by the first microlens. After passing through the beam splitter, it is focused by the second microlens onto the optical disk. The 45° mirror bends the optical beam upward so packaging of the pickup head chip is easier. The return light is collected by the same microlens, reflected by the beam splitter, and focused onto the photodetectors on the silicon substrate. The optical performance of the optical

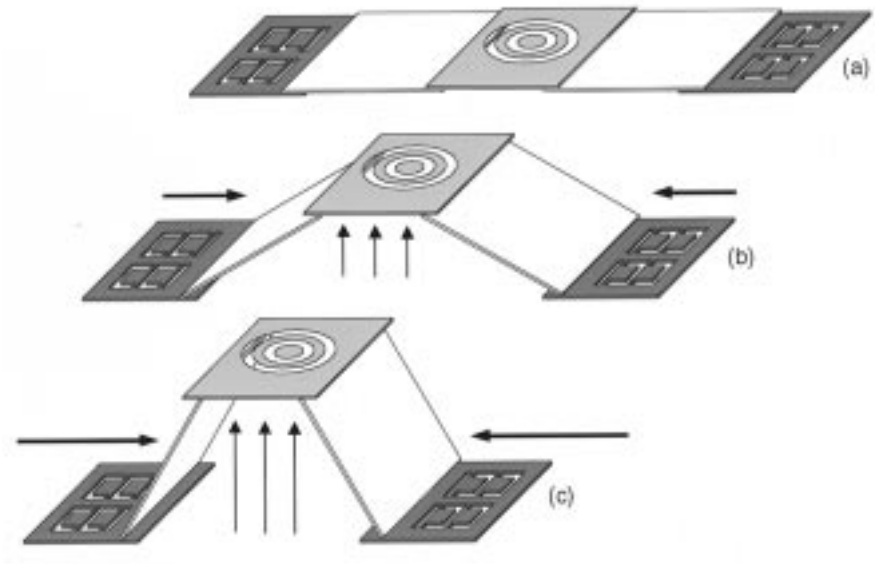

Fig. 25. Schematic illustrating the principle of the self-assembled vertical stage.

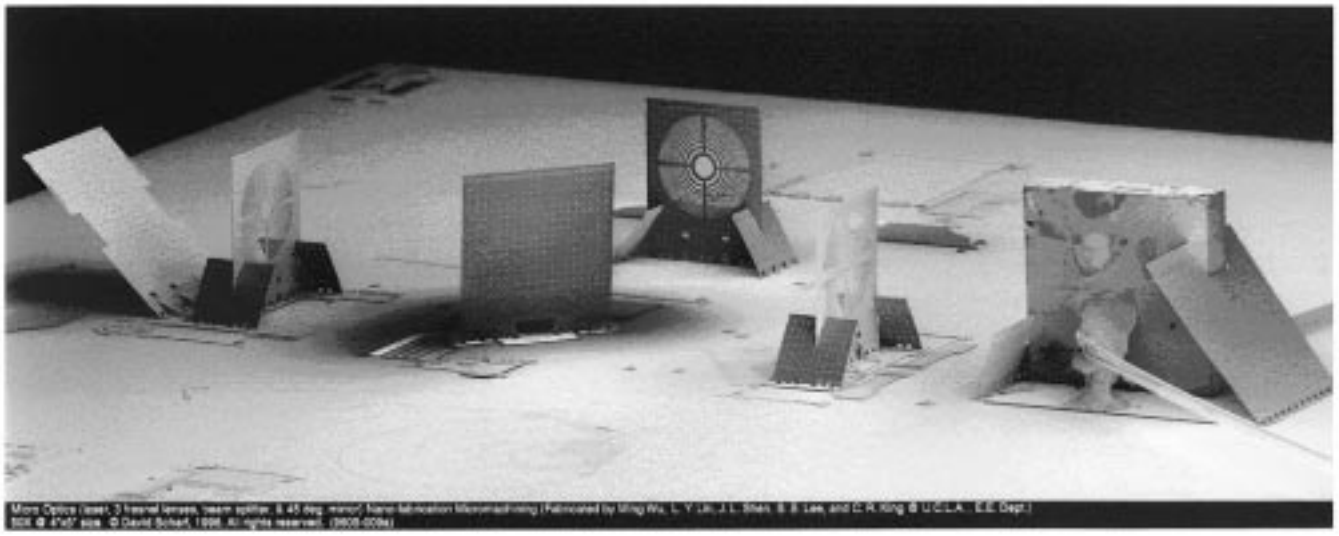

Fig. 26. SEM micrograph of the monolithic optical-disk pickup head. (Photograph by David Scharf.)

pickup head is characterized by the beam profiles at the focal plane and the detector plane, as shown in Fig. 27. For the current demonstration using a 980-nm laser source and the focusing lens with numerical aperture (NA) of 0.17, an FWHM focused spot size of 1.8 μm has been obtained. The spot size can be reduced by employing a shorter wavelength laser and a focusing lens with higher NA.

The monolithic optical-disk pickup head includes the following advantages.

1) *Weight reduction:* The monolithic head is about a thousand times lighter than the conventional heads. Lighter weight allows the head to be accelerated and decelerated much more quickly and can greatly reduce the seek time of optical data storage systems.
2) *Miniaturization:* The size of the pickup head is also dramatically reduced. This opens up the possibility of multiple READ/WRITE heads for the same disk, which can increase the data transfer rate and further reduce the seek time.
3) *Low cost:* The monolithic head is fabricated by a VLSI-like batch fabrication process, potentially at very low cost.
4) *Possible on-chip actuation:* Because the optical disks are removable media, the position and height of the optical head need to be constantly adjusted to maintain focusing and tracking. The tracking function potentially could be integrated on the chip of the pickup head. For example, the 45° upward mirror can be made into a scanning torsion mirror, which

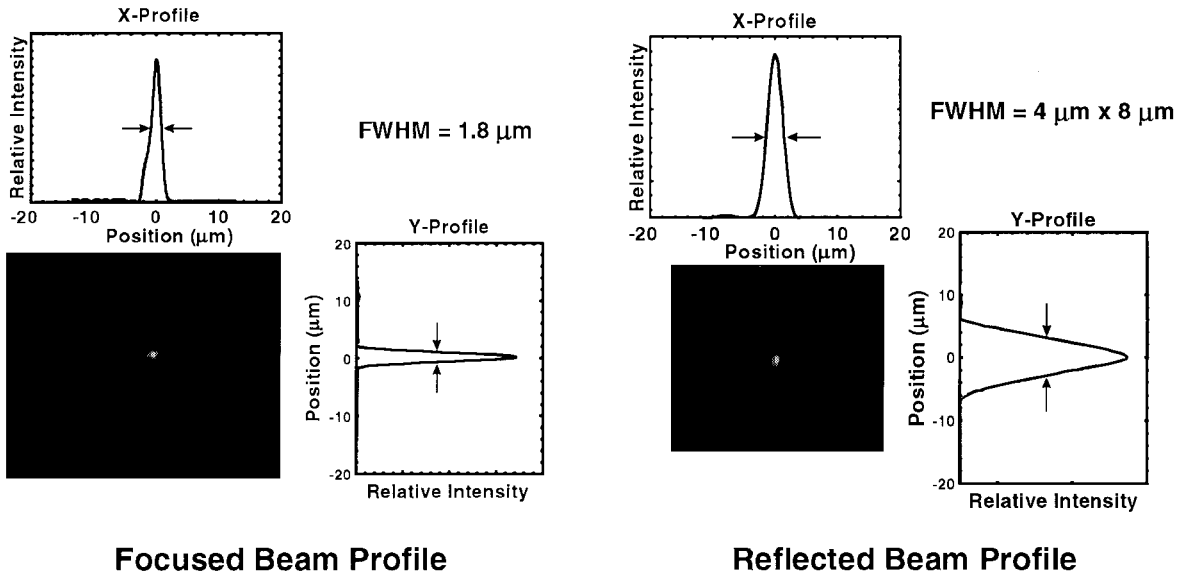

Fig. 27. The profile of the optical beam focused on the surface of the disk and on the photodetector plane.

can scan the focused beam across the tracks of the optical disks.

B. Femtosecond Autocorrelator

Another example of a single-chip microoptical system is the monolithic femtosecond autocorrelator. The autocorrelator is an optical instrument for measuring the duration of ultrashort optical pulses with femtosecond resolution. It consists of an interferometer with a variable delay arm and a nonlinear detector. In principle, the autocorrelator can be made very compact because one femtosecond corresponds to a distance of 0.3 μm. In reality, it is limited by the size of bulk optics, micromechanical stages, and motors, and typical autocorrelators are larger than the size of a shoebox. With FS-MOB, it is possible to monolithically integrate the autocorrelator on a single chip. The SEM micrograph of the autocorrelator is shown in Fig. 28 [64]. It consists of a microactuated translation stage, two beam splitters, and six micromirrors integrated on an Si chip with an area of 4×4.5 mm^2. All the microoptical elements are built monolithically on the Si substrate, with their optical axes parallel to the substrate. A collinear configuration is employed for the first demonstration. Since the FS-MOB can be prealigned during layout of the photomasks, the two optical path lengths are balanced to almost zero initial differential delay. The two beams combine collinearly at the output beam splitter. The variable delay line comprises a two-mirror retroreflector and a microactuated translation stage. It is driven by the SDA's discussed earlier. They have a large travel distance and a fine step size of 27 nm, which corresponds to a temporal resolution of 0.18 fs. We have employed a two-photon-absorption (TPA) photodiode as the nonlinear detector. The semiconductor photodiode can potentially be integrated on the Si substrate. A silicon photodiode can be used for TPA for wavelengths of 1.1–2.2 μm, which covers the spectrum used for fiber communications. Here, we use an InGaP photodiode for detecting the 860-nm femtosecond pulses generated by the Ti:Sapphire laser. The experimental autocorrelation results obtained from the micromachined autocorrelators with TPA photodiode and the conventional autocorrelator with nonlinear crystal are shown in Fig. 29(a) and (b), respectively. Very good agreement has been obtained. The speed of SDA ranges from micrometers/second to 3 mm/s. Therefore, the time required for completing one autocorrelation trace (scan over 1 ps) can be as short as 0.1 s.

C. Fiber-Optic Switches

Free-space fiber-optic switches offer many advantages over conventional waveguide switches. They have lower coupling loss and much smaller cross talk, and are independent of wavelength, polarization, and data format. Both the surface-micromachining and the bulk-micromachining techniques have been used to fabricate fiber-optic switches. A bulk-micromachined 2×2 fiber-optic switch was reported by AT&T Bell Laboratories in 1992 [74]. A (110) silicon wafer is anisotropically etched by EDP to create smooth vertical micromirrors. Very high reflectivity ($>$ 97%) has been achieved for these single crystalline mirrors when coated with Ti/Pt/Au coating. A separate (100) silicon substrate is chemically etched to create four V-grooves and pyramidal holes for aligning fibers and ball lenses. The two wafers are then joined together manually, and external actuators are employed. An insertion loss of 0.7 dB and a switching time of less than 10 ms have been obtained. This switch still requires substantial assembly, however, and the potential cost is high. In the following, we will describe the recent progress in micromachined fiber-optic switches.

1) Surface-Micromachined Fiber-Optic Switches: Under the support of the Defense Advance Research Project Agency, UCLA and the Rockwell Science Center have been investigating manufacturable, low-cost fiber-optic

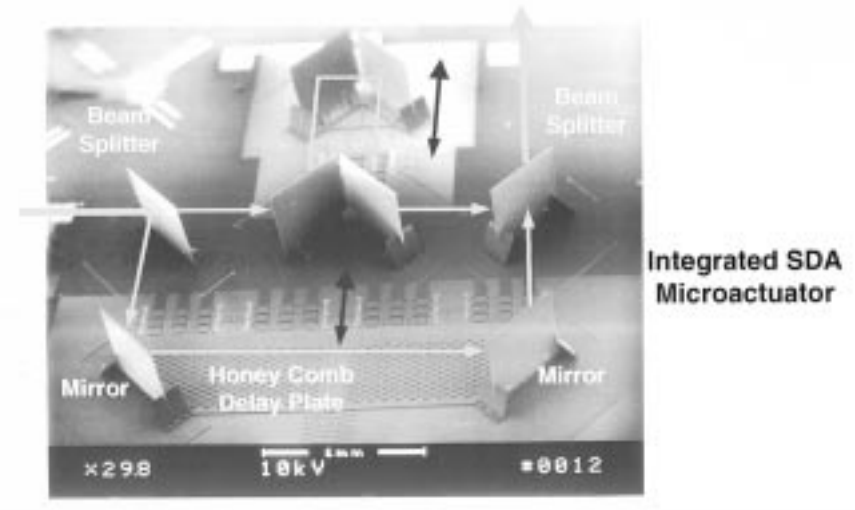

Fig. 28. The schematic and SEM of the femtosecond autocorrelator.

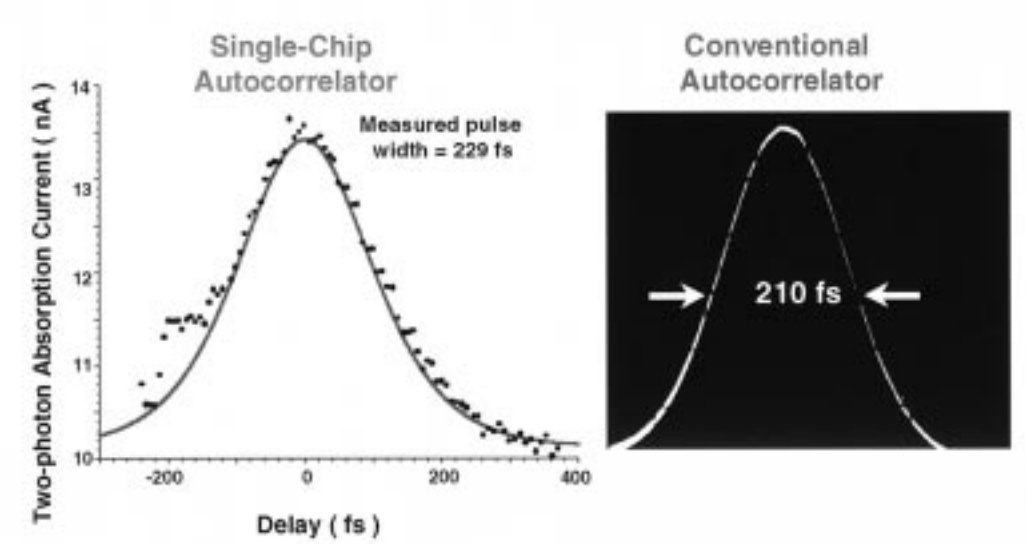

Fig. 29. Experimental autocorrelation traces. (a) Measured by the MEMS autocorrelator with a TPA photodetector. (b) Measured by the conventional autocorrelator with second harmonic generation crystal.

switches using surface-micromachining technologies since 1994 [75]. Surface micromachining offers greater flexibility since it can monolithically integrate various types of three-dimensional microoptical elements with microactuators. The schematic diagram of the switch is shown in Fig. 30. It consists of a movable three-dimensional micromirror, four fiber guiding rails, and microacuators. Depending on the mirror position, light emitted from the input fiber is either transmitted to the opposite fiber or reflected to the orthogonal fiber. By keeping the distance between fibers short, it is possible to achieve low insertion loss without external lenses. For multimode fibers with higher numerical aperture, a semispherical fiber lens can be used to reduce the diffraction loss and to increase the working distance. The mirror is actuated by the SDA microactuators. Instead of using two actuators to move the mirror back and forth, we employ a mechanical flexure spring to pull the SDA back to the center position. This is necessary for the "fail-safe" requirement, i.e., the switch must always return to the bypass state during power failure. Since the SDA force is larger than the spring force, the mirror is moved away by the SDA's when an ac electrical pulse train is applied to the SDA's. The mirror can be maintained at the off-centered position by applying a dc bias to hold the SDA's to the substrate. When the dc voltage is released, or when power failure occurs, the mirror will return to the center position by the spring force. This 2×2 has been fabricated by the three-polysilicon-layer surface-micromachining technology offered at MCNC. The SEM micrograph of the switch is shown in Fig. 31 [63].

The optical performance of the switch has been characterized using four multimode optical fibers with 62.5-μm core diameters. The fiber-to-fiber spacing is 80 μm, and the fiber tip has been melted to form hemispherical microlenses. The

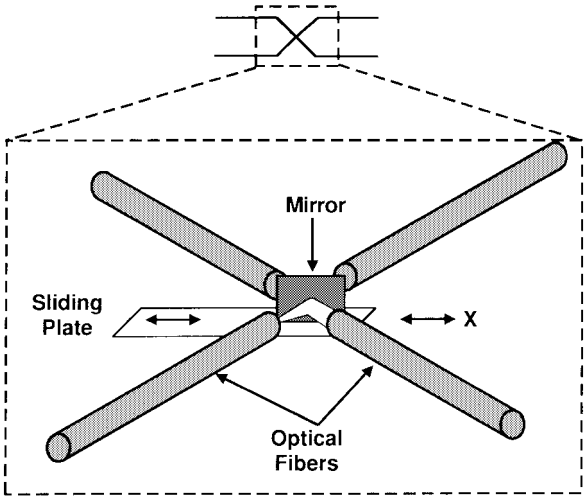

Fig. 30. Schematic of the surface-micromachined fiber-optic switch with a movable micromirror.

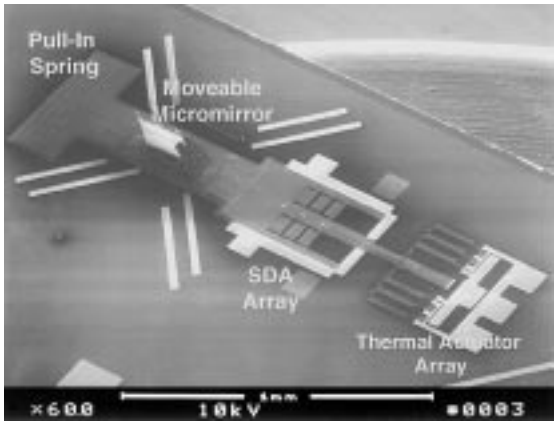

Fig. 31. SEM micrograph of the fiber-optic switch with a movable micromirror.

insertion losses have been characterized to be 1.3 and 1.9 dB for the transmission and reflection modes, respectively. These include the Fresnel loss of the uncoated fibers, which is about 0.4 dB. With further optimization, insertion loss below 1 dB could be achieved. The additional loss of the reflection mode is attributed to the reflectivity of the Au-coated polysilicon mirror ($\sim$ 87%). Higher reflectivity can be obtained by smoothening the surface by the CMP process [34]. The switching time has also been characterized: a switching time of 15 ms is obtained when the SDA is biased at a peak voltage of 100 V at 30 kHz; the mirror returns to the center position in 6 ms when the bias is released.

One of the important, though maybe counterintuitive, advantages of the MEMS fiber-optic switches is their ruggedness against vibration or shocks. Because the inertia force is proportional to the cubic power of linear dimensions (same as the mass), whereas the actuating force is proportional to the linear dimension (for electrostatic force), the inertia force becomes negligible when the device dimension is scaled down to the range of 100 μm [76]. To investigate the robustness of the switch against external vibrations experimentally, we have also performed an *in situ* vibration test when the switch is in operation at Rockwell Science Center. In particular, quantitative measurement in terms of the data bit error rate (BER) has been obtained [63]. For a data rate of 100 Mb/s, error-free operation up to three hours has been obtained for vibrations up to 89 g (equipment limited) and frequencies from 200 Hz to 10 kHz. This corresponds to a BER of less than 10^{-12}. Comparison of the receiving sensitivity with and without vibration shows that there is virtually no effect of vibration of this scale. No mechanical failure was observed throughout the entire test. This confirms the robustness of the MEMS fiber-optic switches.

2) Bulk-Micromachined Fiber-Optic Switches: Recently, several interesting bulk-micromachined fiber-optic switches have been reported. Toshiyoshi and Fujita of the University of Tokyo reported a 2 $\times$ 2 matrix switch using bulk-micromachined torsion mirrors [77]. The torsion mirrors are suspended by thin polysilicon beams over the holes etched through the silicon substrate (Fig. 32). The torsion mirror is arranged at a 45° angle to the fibers. When the mirror is attracted to bend downward by electrostatic force, light is reflected to the orthogonal fibers. Large contrast ratio ($>$ 60 dB), small cross talk ($<$ 60 dB), and an insertion loss of 7.6 dB have been achieved. The matrix geometry is scaleable to larger switches. Marxer *et al.* from the University of Neuchatel have reported bulk-micromachined 2 $\times$ 2 fiber-optic switches using the DRIE process on a silicon-on-insulator wafer (Fig. 33) [13]. The 75-μm-thick silicon layer above SiO_2 is etched through by DRIE. A 2.3-μm-thick vertical mirror as well as the electrostatic microactuator are created by the same etching step. The SiO_2 under the thin beam is then selectively etched to release the mirror and the rotors of the microactuator. In the simplest form of this process, only one lithography step is needed. Switching time below 0.2 ms, coupling loss of 2.5 and 4 dB, and switching voltage of 28 V have been achieved. A similar process has recently been reported by the Michigan group [14].

Miller and Tai of Caltech reported electromagnetically actuated 2 $\times$ 2 fiber-optic switches (Fig. 34) [78]. A 5-μm-thick vertical mirror fabricated by TMAH etching on a (011) silicon substrate is mounted on a suspended silicon plate. The silicon plate is bulk micromachined and connected to the silicon substrate by cantilevers or torsion beams. It is actuated electromagnetically through the interaction of an integrated 70-turn copper coil and an external magnet. A switching time of 10 ms, an insertion loss of 3 dB, and a switching current of 20–30 mA have been achieved. An in-line fiber gate (ON/OFF switch) with similar torsion beam support and electrostatic actuator has been demonstrated by the Nippon Telegraph and Telephone (NTT) group using electroplated Ni as both mirror and microactuator [79].

D. Free-Space Optical Interconnect

A free-space optical interconnect employing vertical-cavity surface emitting lasers (VCSEL's) offers many advantages for high-speed computers and smart pixel ap-

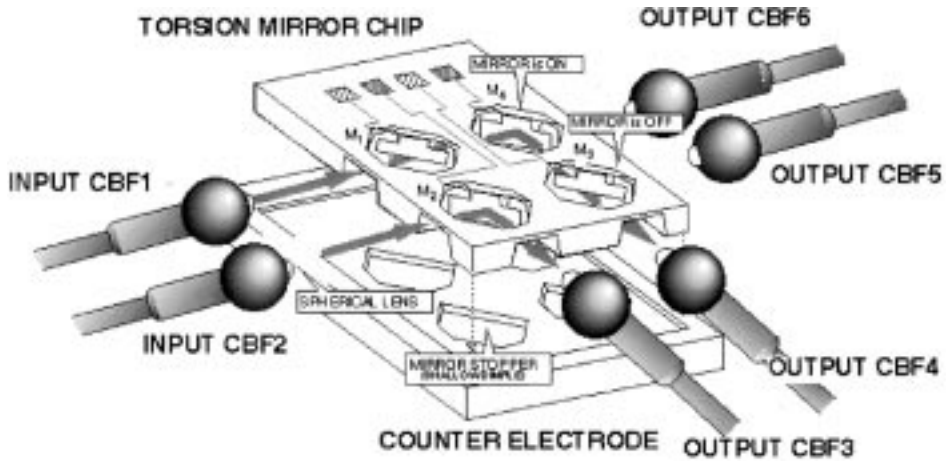

Fig. 32. Schematic of a matrix fiber-optic switch with torsion mirrors [77].

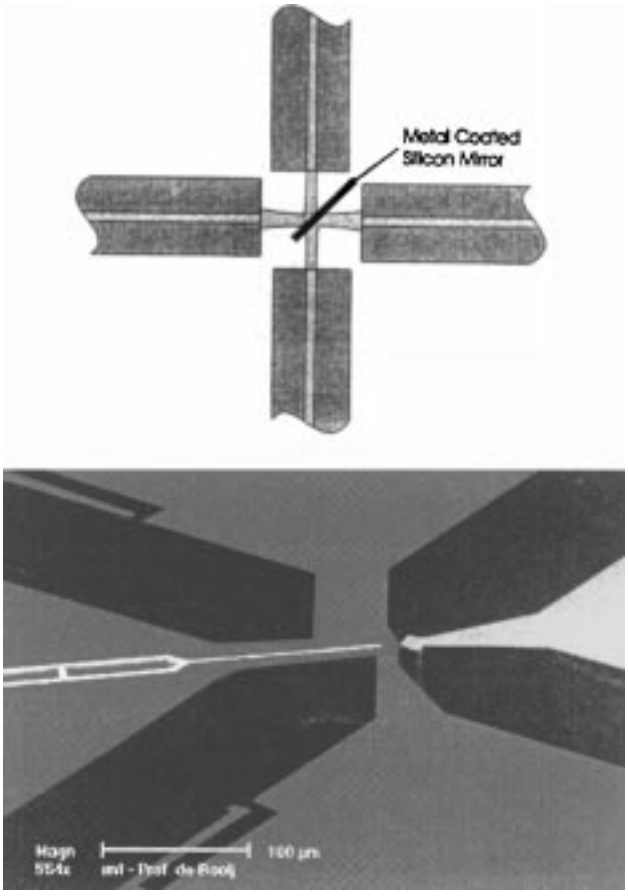

Fig. 33. Schematic of a 2 × 2 fiber-optic switch with vertical mirror fabricated by DRIE [13].

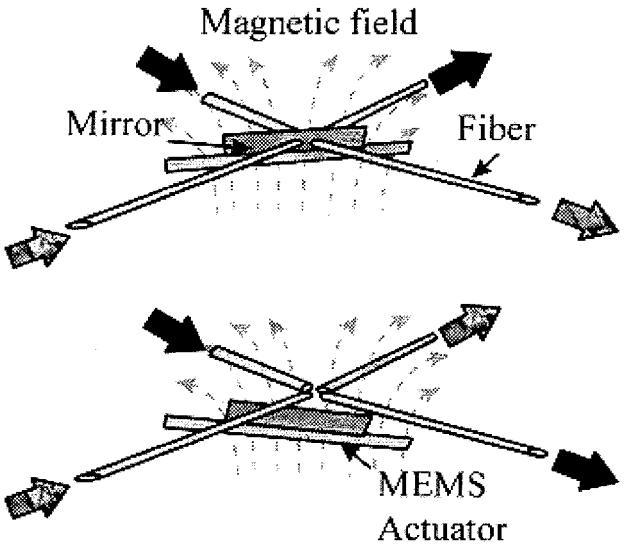

Fig. 34. Schematic of a 2 × 2 fiber-optic switch with (110) etched mirror and electromagnetic actuator [78].

plications. The optical beams emitted from VCSEL's are usually expanded, collimated, or focused by external microlenses. Monolithic integration of fixed refractive [80] and diffractive [81] microlenses on the back side of VCSEL wafers has been demonstrated. In most applications, however, it is desirable to have a dynamically movable microlens on top of the VCSEL to perform dynamic optical alignment, tracking and focusing, continuous optical beam scanning, space division switching, or implementation of reconfigurable optical interconnect.

We have used the surface-micromachining technology to produce a suspended microlens for dynamic alignment in free-space optical interconnect. Fig. 35 shows the SEM micrograph of the suspended scanning microlens [82]. A 670-nm VCSEL is hybrid integrated on the silicon substrate before the microlens is assembled. This suspended microlens can directly collimate or focus light emitted from the VCSEL below it. The microlens is supported by "doubly folded" polysilicon plates. The base of the lens support is hinged to an integrated "XY" translation stage, which is driven by SDA's. The collimated beam can be scanned in two dimensions by moving the suspended microlens. Fig. 36 shows the far-field pattern of the two-dimensional scanning in the $X-Y$ plane. The maximum scanning range of $\pm 8^{\circ}$ has been achieved. A larger scanning angle can be achieved by employing the micro-XY stage with larger travel distances. The structures shown in

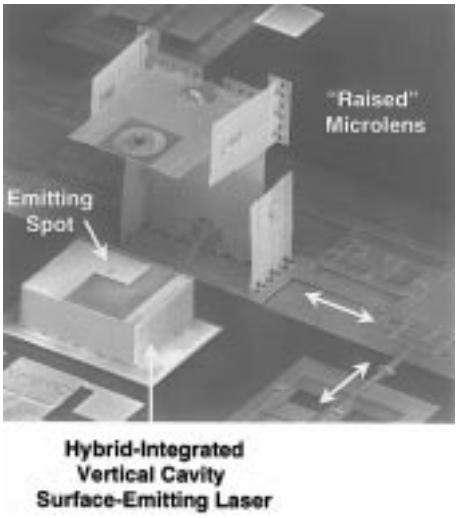

Fig. 35. SEM micrograph of a suspended microlens that can scan in two directions.

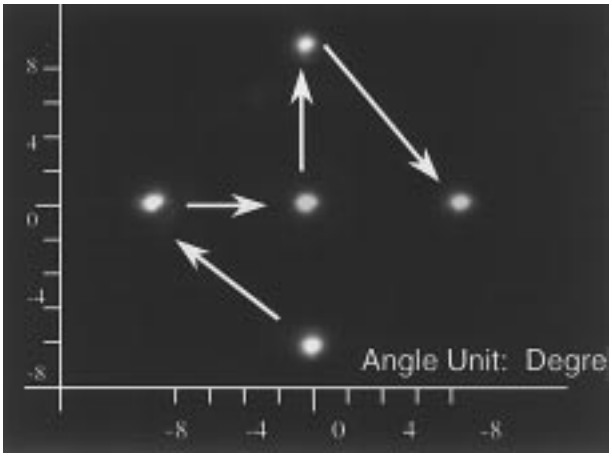

Fig. 36. The measured far-field patterns of the optical beam emitted from a VCSEL and collimated by the suspended microlens as the lens is moved in two in-plane directions.

Fig. 35, however, require substantial manual assembly. The micro-XYZ stage discussed earlier (Fig. 24) eliminates the manual assembly and can achieve dynamic focusing.

V. Other Applications of Micromachined Optics

In addition to the MEMS optical devices discussed here, there are many other bulk- and surface-micromachining devices that have applications in optical and optoelectronic systems. In this section, we will review some important MEMS optical devices and technologies.

A. Spatial Light Modulators and Projection Display

The cantilever beams and torsion mirrors are ideal for implementing spatial light modulators with high brightness and a high contrast ratio [83]. There are two main types of micromechanical spatial light modulators: reflection type and diffractive type. The digital micromirror device is a reflection spatial light modulator [Fig. 37(a)] that can be used in projection display as well as other digital light-processing applications [23]. It is basically a torsion mirror with a $\pm 10^\circ$ rotation angle. The DMD is made by the surface-micromachining process with aluminum structure layers (for electrode, hinge, and mirror) and organic sacrificial materials. All the materials, including the sacrificial layers, are etched by a plasma dry etching process to minimize stiction. In DMD, the hinges and the support mechanical structures are hidden under the mirror. This results in a high contrast ratio ($> 100{:}1$) and greater optical efficiency. Because of its small size, the DMD operates very fast. The switching time is on the order of 10 μs.

The grating light valve (GLV) invented at Stanford University is a diffractive spatial light modulator [84]. It is basically a micromechanical phase grating, as shown in Fig. 37(b). The GLV consists of parallel rows of reflective ribbons. Alternative rows of ribbons can be pulled down electrostatically by one-quarter wavelength, which will send the zeroth-order reflected beam into first-order diffraction beams. The GLV can be configured in various ways to form projection and head-mount displays, which are now pursued by Silicon Light Machine [85]. It shares many advantages of the micromechanical modulators, such as a high contrast ratio and fill factor. Because of the high resonant frequency, it is one of the fastest micromechanical devices. The switching time is only 20 ns [85]. Since the diffraction angle is related to the grating pitch, the GVL is a color-sensitive device. Different pitch gratings can be integrated on the same substrate to form color displays. This will eliminate the need of color filters or color wheels, however, at the expense of sacrificing the fill ratio and, therefore, brightness.

B. Reflection Modulators for Fiber-Optic Communications

Micromechanical light modulators are attractive for low-cost fiber-to-the-home applications [84], [86]. They are a low-cost substitute for an active light source [laser or light emitting diode (LED)] at the subscriber node to provide upstream data transmission. Such modulators could be directly integrated on the driver and receiver circuit chip. The mechanical antireflection switch (MARS) device is shown in Fig. 38 [86]. It is basically a Fabry–Pérot resonator with a movable mirror. The mechanical structure is similar to that of GLV except the it has a flat optical window instead of grating. The reflected light in the surface-normal direction is collected as modulated signal. (The GLV can also be used as a reflection fiber-optic modulator; in fact, it was originally invented as a reflection light modulator [84].) The parallel plate mirrors are spaced by 3 $\lambda_0/4$ (λ_0 is the light wavelength in air), and the reflectivity is high in the absence of bias. The optical membrane is attracted to the substrate by electrostatic force. When the gap between the membrane and the substrate changes from $3\lambda_0/4$ to $\lambda_0/2$, the reflectivity becomes very low due to the destructive interference. A contrast ratio up to 24 dB has been achieved. The resonant frequency of MARS is around 3.5 MHz, and digital modulation of data at 3.5 Mb/s has been demonstrated. In contrast to GLV, however, the MARS device operates in the analog regime (before

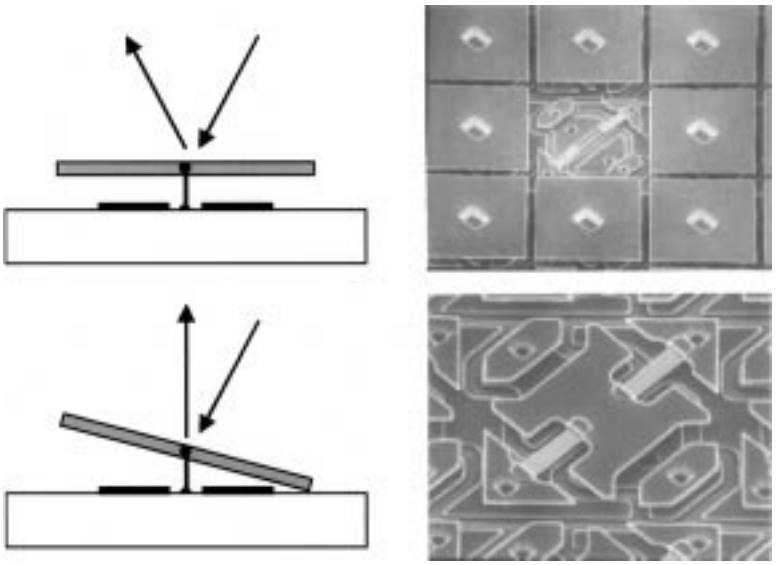

(a)

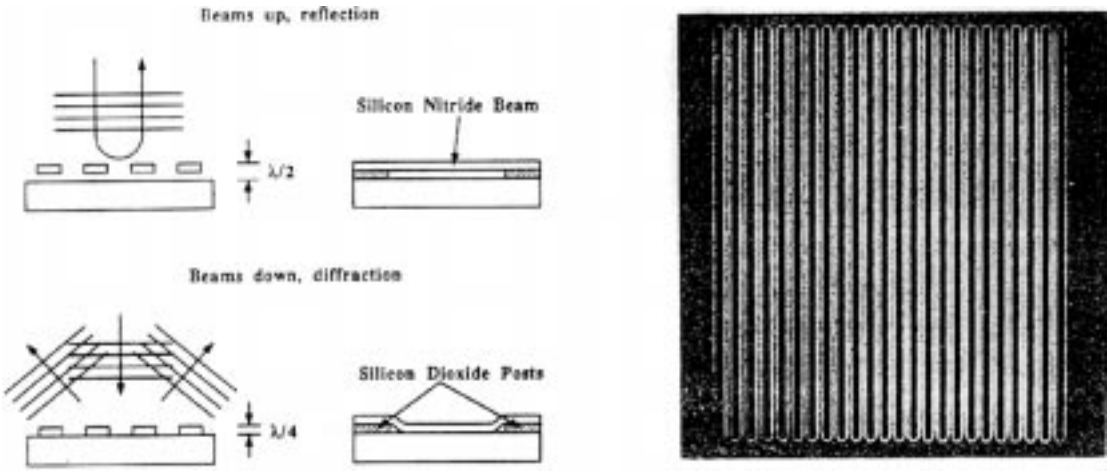

(b)

Fig. 37. Schematic of the (a) DMD [84] and (b) GLV [85] for display applications.

the membrane is "pulled in" toward the substrate), and the mirror plate never makes contact with the substrate. It may have higher reliability because the probability of stiction during operation is much reduced. A similar device has also been reported by researchers from the University of Neuchatel and Ascom [87], [88]. In their device, they use polysilicon membrane as a semitransparent mirror. A photodetector is attached to the modulator to detect the transmitted light (the fiber collects the reflected light). Thus, a full transceiver is realized by this device potentially at very low cost.

C. Optical Scanners

Optical scanning is another fruitful area in which optical MEMS could play a significant role. Many different types of microoptomechanical scanners have been proposed and demonstrated. Most of the scanners are driven at resonant frequency to increase the scanning angle and reduce the driving voltage. Goto reported a two-dimensional optical beam scanner using a single mirror with leaf spring mirror resonator and piezoelectric actuator [89]. By exciting both the bending mode and the torsion mode of the spring leaf-connected resonator, two-dimensional scanning is achieved. A two-dimensional scanning display that combines a seven-element fan-shaped laser array and a surface-micromachined polysilicon microscanner was reported by the Berkeley group (Fig. 39) [90]. The vertical scanning is achieved by simply modulating the individual lasers in the laser array, while the horizontal scanning is achieved by the micromechanical scanner. The microscanner itself is realized by an out-of-plane torsion mirror driven by a comb actuator through microhinges. A resolution of 310 pixels/line has been achieved. A diffraction grating scanner based on the surface-micromachined micromotor is reported by Mehregany and Merat [34]. Motamedi *et al.* of Rockwell reported a micromechanical optical scanner based on bimorph microactuators. A scanning angle of 20° and scan range up to 2 kHz have been achieved with a power less than 1 W [91]. Electromagnetic scanning mirrors have also been reported [92], [93].

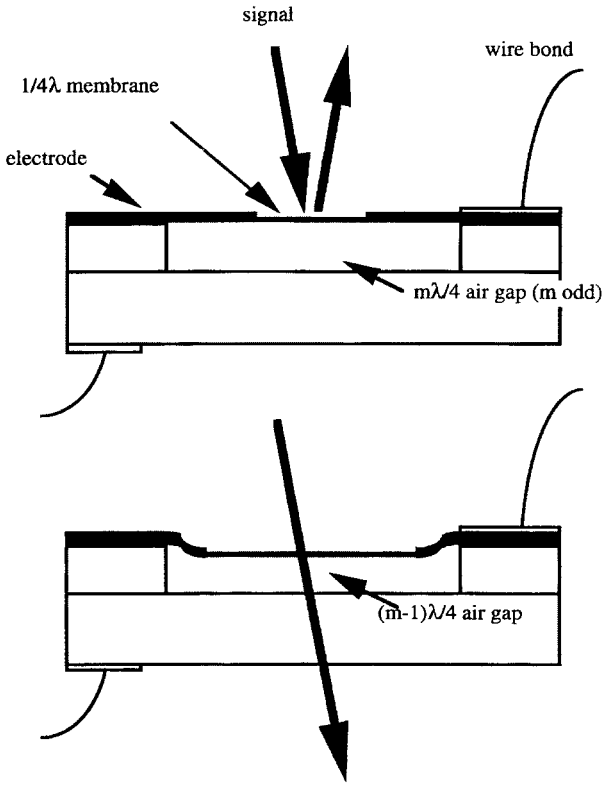

Fig. 38. Schematic of the reflection modulator made by surface micromachining [86].

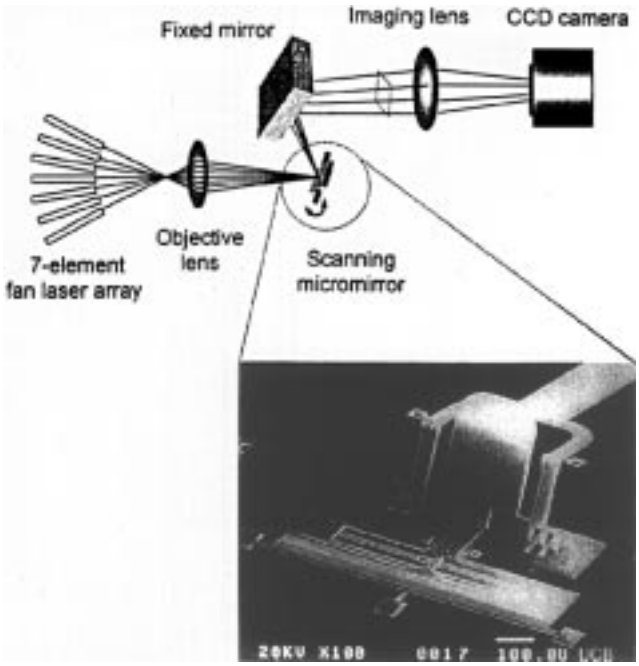

Fig. 39. Schematic of a two-dimensional scanning with a seven-element fan-shaped laser array source and a microscanner [90].

D. Waveguide-Based Microoptical Bench

In addition to free-space applications, waveguide-based optical MEMS devices have also been investigated. A tunable edge emitting laser has been reported by Uenishi *et al.* of NTT [94]. It utilizes an external movable mirror driven by an electroplated Ni comb drive. Discretely wavelength tuning of 20 nm has been demonstrated. Waveguide-based microoptomechanical switches also received a great deal of interest. Ollier and Mottier reported a 1 × 2 waveguide optical switch [95]. The device consists of a movable waveguide and two fixed waveguides, as shown in Fig. 40. The movable waveguide is basically a silica cantilever beam realized by undercutting the silicon below the waveguide. The motion is constrained to the in-plane direction by two flexure beams. The movable waveguide can be pulled toward either fixed waveguide by electrostatic gap-closing actuators. A fiber-to-fiber insertion loss of 3–4 dB, a

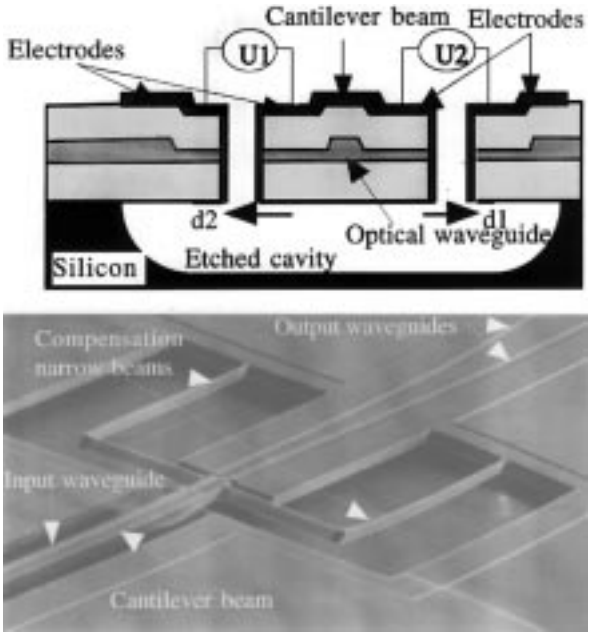

Fig. 40. Schematic and SEM of the movable waveguide switch with integrated electrostatic actuators [95].

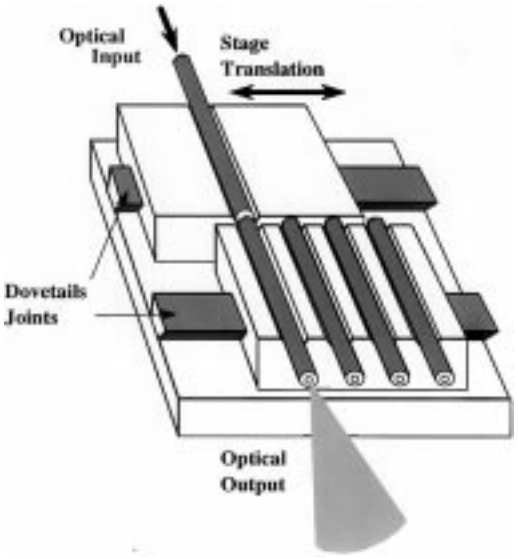

Fig. 41. The electromagnetically actuated 1 × 4 fiber-optic switch realized by bulk micromachining. The input fiber can be moved to line up with one of the output fibers [97].

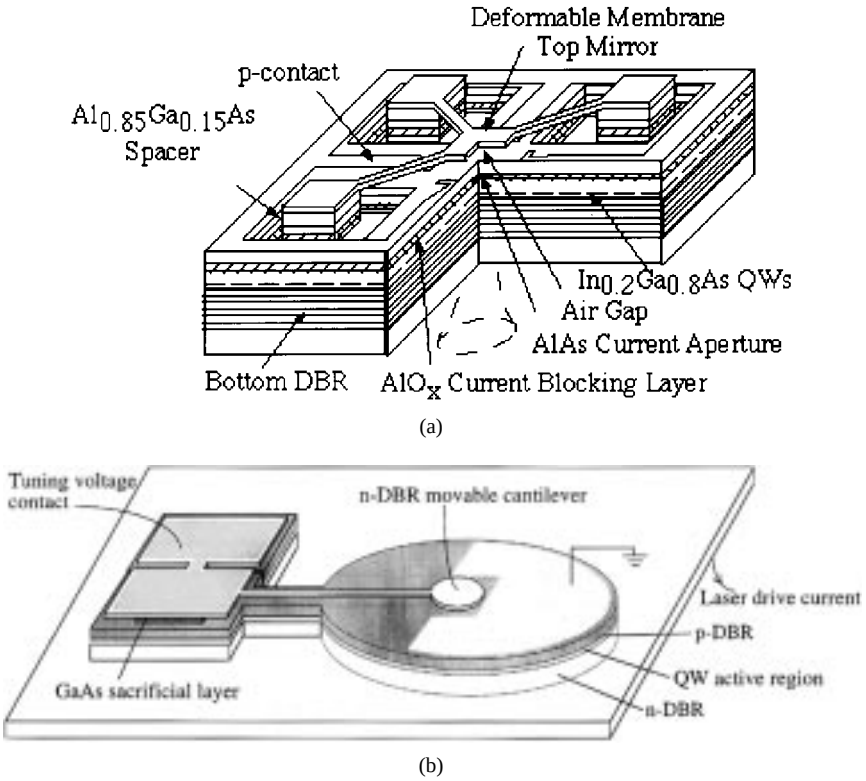

Fig. 42. Schematic of broadly tunable VCSEL's with movable micromechanical top mirrors [102], [103].

switching time of 0.8 ms, and a driving voltage of ± 28 V has been obtained.

Another type of fiber-optic switch involves physical movement of the fiber itself instead of a waveguide. Field *et al.* of Hewlett-Packard [96] reported a 1×2 fiber-optic switch that utilizes an electroplated (LIGA) thermal actuator to move the input fiber between two output fibers. A coupling loss of -5.8 dB and isolation of 66.5 dB have been achieved. Another interesting moving-fiber-optical switch is reported by Gonzales and Collins [97]. The 1×4 switch (Fig. 41) consists of one movable fiber and four fixed fibers. The movable fiber is mounted on a bulk-micromachined translation stage, which is actuated by an electromagnetic actuator. A thin film of paramagnetic material (permalloy) is deposited on the input translation stage, and an external magnetic field is applied to either side of the sliding stage to align the input fiber to the appropriate output fiber. A switching time of 5 ms, an insertion of 1 dB, and a cross talk of -60 dB have been achieved for multimode fibers. One of the major constraints of the waveguide-based fiber-optic switches is that they are mainly constrained to $1 \times n$ switches, and it is more difficult to scale up to larger switches.

E. Micromachined Device on III–V Substrates

Micromachining on III–V materials is a new area that has caught a great deal of interest recently [98]–[101]. The obvious advantage of the III–V substrate is that active optoelectronic devices such as semiconductor lasers, LED's, and photodetectors can be readily integrated with the micromechanical structure. The MEMS technology enables broadly tunable VCSEL's, LED's, photodetectors, and filters to be implemented on III–V compound semiconductor substrates [102]–[106]. Basically, the wavelength tuning range of a Fabry–Pérot cavity with length L and refractive index n can be expressed as

$$\Delta\lambda = \frac{2}{m}\left(L \cdot \Delta n + n \cdot \Delta L\right)$$

where m is the longitudinal mode number. Vertical-cavity lasers can have very large tuning range thanks to the wide mode spacing; however, the effect of index change due to electrooptic or free carrier effect is very weak because of the small cavity length ($L \sim 5$ μm). On the other hand, a very broad tuning range can be obtained by changing the cavity length. This can be accomplished by employing a movable mirror for the cavity. Indeed, a very broad tuning range (> 20 nm) has been demonstrated in such micromachined VCSEL's. Two types of movable mirrors have been investigated: one employs a deformable metal/dielectric/semiconductor membrane [102], the other uses single crystalline semiconductor cantilever beams [103], as shown in Fig. 42(a) and (b), respectively. Broadly tunable LED's, photodetectors, and filters at long wavelength have also been demonstrated [104].

VI. Conclusion

The micromachining technology has opened up many new possibilities for optical and optoelectronic systems. It allows movable micromechanical structures to be inte-

grated monolithically with microoptical elements. The integrated micromechanical device can perform many functions that are not achievable with conventional devices. Optical switches with low loss and high isolation, optical scanners with large scanning angles, high-brightness projection displays, low-cost fiber-optic modulators, broadly tunable semiconductor lasers, photodetectors, and filters have been demonstrated. Single-chip microoptical systems have also been built. Compared with conventional optomechanical devices, the microfabricated devices are smaller, lighter, cheaper, faster, and more rugged and consume less power.

ACKNOWLEDGMENT

The author wishes to thank Dr. L.-Y. Lin of AT&T Research Labs, Dr. J.-L. Shen, L. Fan, S.-S. Lee, C. R. King, J. G. D. Su, and R. Chen for the research work done at UCLA; Prof. K. S. J. Pister for valuable discussions on microhinges; Prof. W. Kaiser, Prof. C. J. Kim, and Dr. M. E. Motamedi for stimulating discussions; the Microelectronics Center at North Carolina for fabrication of the surface-micromachined devices; and members of the Nanofabrication Research Facility at UCLA for help in fabricating the devices.

REFERENCES

[1] S. E. Miller, "Integrated optics: An introduction," *Bell Syst. Tech. J.*, vol. 48, pp. 2059–2068, 1969.
[2] For an overview, see W. S. Trimmer, *Micromechanics and MEMS—Classic and Seminal Papers to 1990.* Piscataway, NJ: IEEE Press, 1997.
[3] For an overview of the recent development in optical MEMS, see *Dig. IEEE/LEOS 1996 Summer Topical Meeting on Optical MEMS and Their Applications*, IEEE, Piscataway, NJ, 1996.
[4] See "Special issue on micro-opto-electro-mechanical systems," *Opt. Eng.*, vol. 36, pp. 1280–1413, May 1997.
[5] K. E. Petersen, "Silicon as a mechanical material," *Proc. IEEE*, vol. 70, pp. 420–457, 1982.
[6] K. E. Bean, "Anisotropic etching of silicon," *IEEE Trans. Electron Devices*, vol. ED-25, pp. 1185–1193, Oct. 1978.
[7] C. H. Henry, G. E. Blonder, and R. F. Kazarinov, "Glass waveguides on silicon for optical packaging," *J. Lightwave Technol.*, vol. 7, pp. 1530–1539, Oct. 1989..
[8] H. Han, J. E. Schramm, J. Mathews, and R. A. Boudreau, "Micromachined silicon structures for single mode passive alignment," in *Proc. SPIE Optoelectronic Packaging*, vol. 2691, pp. 118–123, Feb. 1996.
[9] Y. Uenishi, M. Tsugai, and M. Mehregany, "Micro-opto-mechanical devices fabricated by anisotropic etching of (110) silicon," *J. Micromech. Microeng.*, vol. 5, pp. 305–312, Dec. 1995.
[10] K.-S. Seo, Y.-H. Cho, and S.-K. Youn, "An electrostatically-tunable switching micromirror using (110) silicon wafers," in *Dig. IEEE/LEOS 1996 Summer Topical Meetings on Optical MEM's and Their Applications*, Keystone, CO, 1996, pp. 41–42.
[11] S. Kong, K. Minami, and M. Esashi, "Fabrication of reactive ion etching systems for deep silicon machining," *Trans. Inst. Electr. Eng. Jpn. E*, vol. 117-E, pp. 10–14, Jan. 1997.
[12] E. H. Klaassen, K. Petersen, J. M. Noworolski, J. Logan, N. I. Maluf, J. Brown, C. Storment, W. McCulley, and G. T. A. Kovacs, "Silicon fusion bonding and deep reactive ion etching: A new technology for microstructures," *Sens. Actuators A (Physical)*, vol. A52, pp. 132–139, Mar./Apr. 1996.
[13] C. Marxer, M.-A. Gretillat, N. F. de Rooij, R. Battig, O. Anthamatten, B. Valk, and P. Vogel, "Vertical mirrors fabricated by reactive ion etching for fiber optical switching applications," in *Proc. 10th Workshop Micro Electro Mechanical Systems (MEMS)*, Nagoya, Japan, 1997, pp. 49–54.
[14] W. H. Juan and S. W. Pang, "Batch-micromachined, high aspect ratio Si mirror arrays for optical switching applications," in *Proc. Int. Conf. Solid-State Sensors and Actuators (TRANSDUCERS '97)*, 1997, paper 1A4.09P.
[15] H. C. Nathanson, W. E. Newell, R. A. Wickstrom, and J. R. Davis, Jr., "The resonant gate transistor," *IEEE Trans. Electron Devices*, vol. ED-14, pp. 117–133, 1967.
[16] R. T. Howe and R. S. Muller, "Polycrystalline silicon micromechanical beams," *J. Electrochem. Soc.*, vol. 130, pp. 1420–1423, 1983.
[17] M. Mehregany, K. J. Gabriel, and W. S. N. Trimmer, "Integrated fabrication of polysilicon mechanisms," *IEEE Trans. Electron Devices*, vol. 35, pp. 719–723, 1988.
[18] L. S. Fan, Y. C. Tai, and R. S. Muller, "Integrated movable micromechanical structures for sensors and actuators," *IEEE Trans. Electron Devices*, vol. 35, pp. 724–730, 1988.
[19] ——, "IC-processed electrostatic micro-motors," in *Proc. IEEE Int. Electronic Device Meeting (IEDM)*, San Francisco, CA, 1988, pp. 666–669.
[20] Y. C. Tai, L. S. Fan, and R. S. Muller, "IC-processed micromotors: Design, technology, and testing," in *Proc. IEEE Micro Electro Mechanical Systems (MEMS)*, Salt Lake City, UT, 1989, pp. 1–6.
[21] J. H. Smith, S. Montague, J. J. Sniegowski, J. R. Murray, and P. J. McWhorter, "Embedded micromechanical devices for the monolithic integration of MEMS with CMOS," in *Proc. Int. Electron Devices Meeting*, Washington, D.C., 1995, pp. 609–612.
[22] M. Fischer, M. Nagele, D. Eichner, C. Schollhorn, and R. Strobel, "Integration of surface-micromachined polysilicon mirrors and a standard CMOS process," *Sens. Actuators A (Physical)*, vol. A52, pp. 140–144, 1996.
[23] L. J. Hornbeck, "Digital light processing and MEMS: Timely convergence for a bright future" (abstract), in *Proc. SPIE Symp. Micromachining and Microfabrication*, Austin, TX, Oct. 1995.
[24] K. S. J. Pister, M. W. Judy, S. R. Burgett, and R. S. Fearing, "Microfabricated hinges," *Sens. Actuators A*, vol. 33, pp. 249–256, 1992.
[25] Y. Fukuta, D. Collard, T. Akiyama, E. H. Yang, and H. Fujita, "Microactuated self-assembling of 3D polysilicon structures with reshaping technology," in *Proc. IEEE Micro Electro Mechanical Systems (MEMS)*, Nagoya, Japan, 1977, pp. 477–481.
[26] P. W. Green, R. R. A. Syms, and E. M. Yeatman, "Demonstration of three-dimensional microstructure self-assembly," *J. Microelectromech. Syst.*, vol. 4, pp. 170–176, 1995.
[27] E. Smela, L. Inganas, and I. Lundstrom, "Controlled folding of micrometer-size structures," *Science*, vol. 268, pp. 1735–1738.
[28] M. C. Wu, L. Y. Lin, S. S. Lee, and K. S. J. Pister, "Micromachined free-space integrated micro-optics," *Sens. Actuators: A (Physical)*, vol. 50, pp. 127–134, 1995.
[29] M. E. Motamedi, M. P. Griswold, and R. E. Knowlden, "Silicon microlenses for enhanced optical coupling to silicon focal planes," in *Proc. SPIE*, vol. 1544, 1991, pp. 22–32.
[30] K. Rastani, A. Marrakchi, S. F. Habiby, W. M. Hubbard, H. Gilchrist, and R. E. Nahory, "Binary phase Fresnel lenses for generation of two-dimensional beam arrays," *Appl. Opt.*, vol. 30, no. 11, pp. 1347–1354, 1991.
[31] M. E. Motamedi, M. C. Wu, and K. S. J. Pister, "Micro-opto-mechanical devices and on-chip optical processing," *Opt. Eng.*, vol. 36, pp. 1282–1297, 1997.
[32] L. Y. Lin, S. S. Lee, K. S. J. Pister, and M. C. Wu, "Three-dimensional micro-Fresnel optical elements fabricated by micromachining technique," *Electron. Lett.*, vol. 30, pp. 448–449, 1994.
[33] ——, "Micro-machined three-dimensional micro-optics for integrated free-space optical system," *IEEE Photon. Technol. Lett.*, vol. 6, pp. 1445–1447, 1994.
[34] A. A. Yasseen, S. W. Smith, M. Mehregany, and F. L. Merat, "Diffraction grating scanners using polisilicon micromotors," in *Proc. IEEE Micro Electro Mechanical Systems*, Amsterdam, The Netherlands, Jan. 29–Feb. 2, 1995, pp. 175–180.
[35] H. Sankur, E. Motamedi, R. Hall, W. J. Gunning, and M. Khoshnevisan, "Fabrication of refractive microlens arrays," in *Proc. SPIE Micro-Optics/Micromechanics and Laser Scanning and Shaping*, vol. 2383, 1995, pp. 179–183.
[36] T. R. Jay, M. B. Stern, and R. E. Knowlden, "Effect of refractive microlens array fabrication parameters on optical quality," in *Proc. SPIE Miniature and Micro-Optics*, vol. 1751, 1992, pp. 236–245.
[37] Z. D. Popovic, R. A. Sprague, and G. A. Neville Connell,

"Technique for monolithic fabrication of microlens arrays," *Appl. Opt.*, vol. 27, no. 7, pp. 1281–1284, 1988.
[38] N. J. Phillips and C. A. Barnett, "Micro-optic studies using photopolymers," in *Proc. SPIE Miniature and Micro-Optics*, vol. 1544, 1991, pp. 10–21.
[39] C. R. King, L. Y. Lin, and M. C. Wu, "Monolithically integrated refractive microlens standing perpendicular to the substrate," in *Proc. SPIE Photonics West'96*, San Jose, CA, Jan. 1996, vol. 2687, pp. 123–130.
[40] P. Beckmann and A. Spizzichino, *The Scattering of Electromagnetic Waves From Rough Surface.* Norwood, MA: Artech House, 1987, ch. 3–5.
[41] S. S. Lee, L. Y. Lin, and M. C. Wu, "Surface-micromachined free-space micro-optical systems containing three-dimensional micro-gratings," *Appl. Phys. Lett.*, vol. 67, pp. 2135–2137, 1995.
[42] ——, "Distributed feedback lasers integrated with micromachined wavelength-meter for dense WDM systems," in *Proc. 1996 Conf. Lasers and Electro-Optics (CLEO)*, Anaheim, CA, June 3–7, 1996, paper CFG2.
[43] M. H. Kiang, J. T. Nee, K. Y. Lau, and R. S. Muller, "Surface-micromachined diffraction gratings for scanning spectroscopic applications," in *Proc. Int. Conf. Solid-State Sensors and Actuators (TRANSDUCERS '97)*, 1997, pp. 343–345.
[44] W. C. Tang, T. C. H. Nguyen, and R. T. Howe, "Laterally driven polysilicon resonant microstructures," in *Proc. Micro Electro Mechanical Systems (MEMS)*, 1989, pp. 53–59.
[45] W. C. Tang, T. C. H. Nguyen, M. W. Judy, and R. T. Howe, "Electrostatic-comb drive of lateral polysilicon resonators," *Sensors Actuators A (Physical)*, vol. A21, pp. 328–331, 1990.
[46] M. T. Ching, R. A. Brennen, and R. M. White, "Microfabricated optical chopper," in *Proc. SPIE*, 1993, vol. 1992, pp. 40–46.
[47] M. H. Kiang, O. Solgaard, R. S. Muller, and K. Lau, "Micromachined polysilicon microscanners for barcode readers," *IEEE Photon. Technol. Lett.*, vol. 8, pp. 1707–1709, 1996.
[48] W. S. N. Trimmer and K. J. Gabriel, "Design considerations for a practical electrostatic micro-motor," *Sens. Actuators*, vol. 11, pp. 189–206, 1987.
[49] P. B. Chu, P. R. Nelson, M. I. Tachiki, and K. S. J. Pister, "Dynamics of polysilicon parallel-plate electrostatic actuators," *Sens. Actuators A (Physical)*, vol. A52, p. 216–220, 1996.
[50] A. P. Lee and A. P. Pisano, "Polysilicon angular microvibromotors," *J. Microelectromech. Syst.*, vol. 1, pp. 70–76, 1992.
[51] M. M. Daneman, N. C. Tien, O. Solgaard, A. P. Pisano, K. Y. Lau, and R. S. Muller, "Linear microvibromotor for positioning optical components," *J. Microelectromech. Syst.*, vol. 5, pp. 159–165, 1996.
[52] M. J. Daneman, O. Solgaard, N. C. Tien, K. Y. Lau, and R. S. Muller, "Laser-to-fiber coupling module using a micromachined alignment mirror," *IEEE Photon. Technol. Lett.*, vol. 8, pp. 396–398, 1996.
[53] R. Yeh, E. J. J. Kruglick, and K. S. J. Pister, "Surface-micromachined components for articulated microrobots," *J. Microelectromech. Syst.*, vol. 5, pp. 10–17, 1996.
[54] N. R. Tas, A. H. Sonnenberg, A. F. M. Sander, and M. C. Elwenspoek, "Surface micromachined linear electrostatic stepper motor," in *Proc. IEEE Micro Electro Mechanical Systems (MEMS)*, 1997, pp. 215–220.
[55] E. J. Garcia and J. J. Sniegowski, "Surface micromachined microengine," *Sens. Actuators A (Physical)*, vol. A48, pp. 203–214, 1995.
[56] J. J. Sniegowski and E. J. Garcia, "Surface-micromachined gear trains driven by an on-chip electrostatic microengine," *IEEE Electron Device Lett.*, vol. 17, pp. 366–368, 1996.
[57] J. J. Sniegowski, S. L. Miller, G. F. LaVigne, M. S. Rodgers, and P. J. McWhorter, "Monolithic geared-mechanisms driven by a polysilicon surface-micromachined on-chip electrostatic microengine," in *Proc. Solid State Sensor and Actuator Workshop*, Hilton Head, SC, 1996, pp. 178–182.
[58] J. J. Sniegowski and E. J. Garcia, "Microfabricated actuators and their application to optics," in *Proc. SPIE*, vol. 2383, 1995, pp. 46–64.
[59] T. Akiyama and K. Shono, "Controlled stepwise motion in polysilicon microstructures," *J. Microelectromech. Syst.*, vol. 2, pp. 106–110, 1993.
[60] T. Akiyama, D. Collard, and H. Fujita, "Scratch drive actuator with mechanical links for self-assembly of three-dimensional MEMS," *J. Microelectromech. Syst.*, vol. 6, pp. 10–17, 1997.
[61] P. Langlet, D. Collard, T. Akiyama, and J. Fujita, "A quantitative analysis of scratch drive actuation for integrated X/Y motion system," in *Proc. Int. Conf. Solid-State Sensors and Actuators (TRANSDUCERS 97)*, 1997, paper 3A2.01.
[62] L. Fan, M. C. Wu, K. Choquette, and M. H. Crawford, "Self-assembled microactuated XYZ stages for optical scanning and alignment," in *Proc. 1997 Int. Conf. Solid-State Sensors and Actuators (TRANSDUCERS 97)*, 1997, paper 2A2.01.
[63] S. S. Lee, E. Motamedi, and M. C. Wu, "Surface-micromachined free-space fiber optic switches with integrated microactuators for optical fiber communication systems," in *Proc. 1997 Int. Conf. Solid-State Sensors and Actuators (TRANSDUCERS 97)*, 1997, paper 1A4.07P.
[64] G. D. Su, L. Y. Lin, and M. C. Wu, "Single-chip femtosecond autocorrelator realized by surface-micromachined integrated optics," in *Proc. Conf. Lasers and Electro-Optics (CLEO)*, Baltimore, MD, 1997, paper CWL2.
[65] H. Guckel, J. Klein, T. Christenson, K. Skrobis, M. Laudon, and E. G. Lovell, "Thermalmagnetic metal flexure actuators," in *Proc. IEEE Solid State Sensors and Actuators Workshop*, Hilton Head, SC, 1992, p. 73.
[66] J. H. Comtois, V. M. Bright, and M. W. Phipps, "Thermal microactuators for surface-micromachining processes," in *Proc. SPIE*, 1995, vol. 2642, pp. 10–21.
[67] J. H. Comtois and V. M. Bright, "Applications for surface-micromachined polysilicon thermal actuators and arrays," *Sens. Actuators A (Physical)*, vol. A58, pp. 19–25, 1997.
[68] L. Y. Lin, S. S. Lee, and M. C. Wu, "45° out of plane beam steering optics for vertical alignment in free-space micro-optical bench," in *Proc. Conf. Lasers and Electro-Optics (CLEO)*, Anaheim, CA, 1996, paper CFC5.
[69] L. Y. Lin, J. L. Shen, S. S. Lee, and M. C. Wu, "Surface-micromachined micro-XYZ stages for free-space micro-optical bench," *IEEE Photon. Technol. Lett.*, vol. 9, pp. 345–347, Mar. 1997.
[70] Y. Xu, N. C. MacDonald, and S. A. Miller, "Integrated micro-scanning tunneling microscope," *Appl. Phys. Lett.*, vol. 67, pp. 2305–2307, 1995.
[71] A. Selvakumar, K. Najafi, W. H. Juan, and S. Peng, "Vertical comb array microactuators," in *Proc. IEEE Workshop Micro Electro Mechanical Systems*, Amsterdam, The Netherlands, 1995, pp. 43–48.
[72] L. Fan and M. C. Wu, "Self-assembled micro-XYZ stages for moving micro-ball lenses," presented at the Int. Conf. on Optical MEMS and Their Applications, Nara, Japan, Nov. 1997.
[73] L. Y. Lin, J. L. Shen, S. S. Lee, and M. C. Wu, "Realization of novel monolithic free-space optical disk pickup heads by surface micromachining," *Opt. Lett.*, vol. 21, no. 2, pp. 155–157, Jan. 15, 1996.
[74] M. F. Dautartas, A. M. Benzoni, Y. C. Chen, G. E. Blonder, B. H. Johnson, C. R. Paola, E. Rice, and Y. H. Wong, "A silicon-based moving mirror optical switch," *J. Lightwave Technol.*, vol. 8, pp. 1078–1085, 1992.
[75] S. S. Lee, L. Y. Lin, and M. C. Wu, "Surface-micromachined free-space fiber optic switches," *Electron. Lett.*, vol. 31, no. 17, pp. 1481–1482, Aug. 1995.
[76] W. S. N. Trimmer, "Microrobots and micromechanical systems," *Sens. Actuators*, vol. 19, pp. 267–287, 1989.
[77] H. Toshiyoshi and H. Fujita, "Electrostatic micro torsion mirrors for an optical switch matrix," *J. Microelectromech. Syst.*, vol. 5, pp. 231–237, 1996.
[78] R. A. Miller, Y. C. Tai, G. Xu, J. Bartha, and F. Lin, "An electromagnetic MEMS 2×2 fiber optic bypass switch," in *Proc. Int. Conf. Solid-State Sensors and Actuators (TRANSDUCERS '97)*, 1997, pp. 89–92.
[79] E. Hashimoto, Y. Uenishi, K. Honma, and S. Nagaoka, "Micro-optical gate for fiber optic communications," in *Proc. Int. Conf. Solid-State Sensors and Actuators (TRANSDUCERS '97)*, 1997, pp. 331–334.
[80] E. M. Strzelecka, G. D. Robinson, M. G. Peters, F. H. Peters, and L. A. Coldren, "Monolithic integration of vertical-cavity laser diodes with refractive GaAs microlenses," *Electron. Lett.*, vol. 31, pp. 724–725, 1995.
[81] T. Du, M. E. Warren, J. R. Wendt, G. A. Vawter, S. P. Kilcoyne, K. L. Lear, R. P. Schneider, A. J. Howard, R. F. Carson, and J. C. Zolper, "Directional beam control using on/off-axis high-efficiency diffractive optics integrated on substrate-emitting

vertical cavity lasers," in *Proc. Conf. Lasers and Electro-Optics (CLEO'95)*, Baltimore, MD, 1995, pp. 195–196.
[82] L. Fan, M. C. Wu, and K. D. Choquette, "Two-dimensional scanning microlenses for vertical cavity surface-emitting lasers," in *1997 Conf. of Lasers and Electro-Optics (CLEO)*, Baltimore, MD, May 18–23, 1997, paper CME2.
[83] K. E. Petersen, "Silicon torsional scanning mirror," *IBM J. Res. Develop.*, vol. 24, pp. 631–637, 1980.
[84] O. Solgaard, F. S. A. Sandejas, and D. M. Bloom, "Deformable grating optical modulator," *Opt. Lett.*, vol. 17, pp. 688–690, 1992.
[85] D. M. Bloom, "The grating light valve: Revolutionizing display technology," in *Proc. SPIE*, 1997.
[86] J. A. Walker, K. W. Goossen, and S. C. Arney, "Fabrication of a mechanical antireflection switch for fiber-to-the-home systems," *J. Microelectromech. Syst.*, vol. 5, pp. 45–51, 1996.
[87] C. Marxer, M. A. Gretillat, V. P. Jaecklin, R. Baettig, O. Anthamatten, P. Vogel, and N. F. de Rooij, "Megahertz opto-mechanical modulator," *Sens. Actuators A (Physical)*, vol. A52, pp. 46–50, 1996.
[88] O. Anthamatten, R. K. Battig, B. Valk, P. Vogel, C. Marxer, M. Gretillat, and N. F. de Rooij, "Packaging of a reflective optical duplexer based on silicon micromechanics," in *Proc. IEEE/LEOS 1996 Summer Topical Meetings on Optical MEM's and Their Applications*, Piscataway, NJ, 1996, pp. 61–62.
[89] H. Goto, "Si micromachined 2D optical scanning mirror and its application to scanning sensors," in *Proc. IEEE/LEOS 1996 Summer Topical Meetings on Optical MEM's and Their Applications*,, Piscataway, NJ, 1996, pp. 17–18.
[90] D. A. Francis, M.-H. Kiang, O. Solgaard, K. Y. Lau, R. S. Muller, and C. J. Chang-Hasnain, "Compact 2D laser beam scanner with fan laser array and Si micromachined microscanner," *Electron. Lett.*, vol. 33, pp. 1143–1145, 1997.
[91] M. E. Motamedi, S. Park, A. Wang, M. S. Dadkhah, A. P. Andrews, H. O. Marcy, M. Khoshnevisan, A. E. Chiou, R. J. Huhn, C. F. Sell, and J. G. Smits, "Development of micro-electro-mechanical optical scanner," *Opt. Eng.*, vol. 36, pp. 1346–1353, 1997.
[92] R. A. Miller and T. Yu-Chong, "Micromachined electromagnetic scanning mirrors," *Opt. Eng.*, vol. 36, pp. 1399–1407, 1997.
[93] J. W. Judy, R. S. Muller, and H. H. Zappe, "Magnetic microactuation of polysilicon flexure structures," *J. Microelectromech. Syst.*, vol. 4, pp. 162–169, 1995.
[94] Y. Uenishi, K. Honma, and S. Nagaoka, "Tunable laser diode using a nickel micromachined external mirror," *Electron. Lett.*, vol. 32, no. 13, pp. 1207–1208, June 20, 1996.
[95] E. Ollier and P. Mottier, "Integrated electrostatic micro-switch for optical fiber networks driven by low voltage," *Electron. Lett.*, vol. 32, pp. 2007–2009, 1996.
[96] L. A. Field, D. L. Burriesci, P. R. Robrish, and R. C. Ruby, "Micromachined 1*2 optical-fiber switch," *Sens. Actuators A (Physical)*, vol. A53, pp. 311–316, 1996.
[97] C. Gonzalez and S. D. Collins, "Magnetically actuated fiber-optic switch with micromachined positioning stages," *Opt. Lett.*, vol. 22, pp. 709–711, 1997.
[98] Z. L. Zhang and N. C. MacDonald, "Fabrication of submicron high-aspect-ratio GaAs actuators," *J. Microelectromech. Syst.*, vol. 2, pp. 66–73, 1993.
[99] K. Hjort, J. Soderkvist, and J.-A. Schweitz, "Gallium arsenide as a mechanical material," *J. Micromech. Microeng.*, vol. 4, pp. 1–13, 1994.
[100] Y. Uenishi, H. Tanaka, and H. Ukita, "Characterization of AlGaAs microstructure fabricated by AlGaAs/GaAs micromachining," *IEEE Trans. Electron Devices*, vol. 41, pp. 1778–1783, Oct. 1994.
[101] K. Hjort, "Sacrificial etching of III–V compounds for micromechanical devices," *J. Micromech. Microeng.*, vol. 6, pp. 370–375, 1996.
[102] F. Sugihwo, M. C. Larson, J. S. Harris, Jr., "Low threshold continuously tunable vertical-cavity surface-emitting lasers with 19.1 nm wavelength range," *Appl. Phys. Lett.*, vol. 70, pp. 547–549, 1997.
[103] M. Y. Li, W. Yuen, G. S. Li, and C. J. Chang-Hasnain, "High performance continuously tunable top-emitting vertical cavity laser with 20 nm wavelength range," *Electron. Lett.*, vol. 33, pp. 1051–1052, 1997.
[104] G. L. Christenson, A. T. T. D. Tran, Z. H. Zhu, Y. H. Lo, M. Hong, J. P. Mannaerts, and R. Bhat, "Long-wavelength resonant vertical-cavity LED/photodetector with a 75-nm tuning range," *IEEE Photon. Technol. Lett.*, vol. 9, pp. 725–727, 1997.
[105] E. C. Vail, M. S. Wu, G. S. Li, L. Eng, and C. J. Chang-Hasnain, "GaAs micromachined widely tunable Fabry–Pérot filters," *Electron. Lett.*, vol. 31, pp. 228–229, 1995.
[106] M. C. Larson and J. S. Harris, Jr., "Broadly-tunable resonant-cavity light-emitting diode," *IEEE Photon. Technol. Lett.*, vol. 7, pp. 1267–1269, 1995.

Ming C. Wu (Member, IEEE) received the M.S. and Ph.D. degrees in electrical engineering from the University of California, Berkeley, in 1985 and 1988, respectively.

From 1988 to 1992, he was a member of the Technical Staff at AT&T Bell Laboratories, Murray Hill, NJ, where he conducted research in high-speed semiconductor lasers and opto-electronics. In 1993, he joined the Faculty of the Electrical Engineering Department of the University of California, Los Angeles, where he currently is a Professor. He also is the Director of the MURI Center on RF Photonic Materials and Devices sponsored by the Office of Naval Research. His current research interests include micromachined microoptics, optical microelectromechanical systems (MEMS), free-space integrated optics, ultrafast integrated optoelectronics, microwave photonics, high-power photodetectors, semiconductor lasers, and optical interconnect. He has published more than 85 journal papers, 120 conference papers, and one book chapter, and has received eight U.S. patents.

Dr. Wu is a member of the American Physical Society, the Optical Society of America, the International Union of Radio Science, and Eta Kappa Nu. He was General Cochair of the IEEE LEOS Summer Topical Meeting in 1995 (RF Optoelectronics) and 1996 (Optical MEMS) and Program Committee Chair of the 1997 IEEE LEOS Topical Meeting on Optical MEMS. He also served on the Program Committee of the Conference on Lasers and Electro-Optics from 1996 to 1998 and IEDM in 1996. He received the Packard Foundation Fellowship in 1992 and the Meritorious Conference Paper Award of the 1994 Government Microcircuit Applications Conference.